令和元年度修士学位論文

Short-cavity Mode-locked Fiber Laser Using Saturable Absorber Incorporating CNT@BNNT

(CNT@BNNT 可飽和吸収素子を使用した短共振器モード同期ファイバーレーザー)

袁　鵬涛

指導教員　山下真司　教授

東京大学大学院　工学研究科
電気系工学専攻　37-175094

令和元年　8 月 15 日

Table of contents

Chapter 1

Introduction

1.1 Background

The idea of "trapping" light inside cladded glass fibers was born in the 1950s [1, 2] during the development of endoscope application. In 1966, C. Kao et al. Suggested the possibility of optical fiber as a low loss transmission pass theoretically [3]. Since then, the research on optical fibers developed rapidly. The losses of silica fibers were reduced to below 20 dB/km [4] in 1970. And further progress on fabrication technology [5] has made the loss of 0.2 dB/km in the $1.55\,\mu m$ wavelength region [6]. Nowadays, the loss of fiber has come close to the theoretical which is mainly limited by Rayleigh scattering.Meanwhile, with the development of Erbium doped fiber amplifier (EDFA), and related techonologies such as high power laser diode (LD) pump source, wavelength division multiplexing (WDM) coupler, optical isolator and so on, the transmission capacity per fiber has dramatically increased, which leaded the building and popularizing of modern long distance communication system based on $1.55\,\mu m$ wavelength region.

Although optical fiber has been widely known as transmission pass of light communication, its characteristics have been researched and applied in other fields. Optical fibers can be used as strain / temperature sensors, fiber Bragg grating (FBG) can be used as wavelength filter [7–9]. In the 1970s, advent of the field of nonlinear fiber optics also broaden the view of fiber application [10]. In 1973, it was suggested that optical fibers can support soliton-like pulses as a result of an interplay between the fiber disperion and nonlinear effect [11], and the experiment in 1980 confirmed the existence of optical soliton from an optical-fiber-incoporated laser [12]. From then on, a large number of researches has been advancing the generation and control of ultrashort optical pulses. These introduced optical fiber into ultrafast optics which is an important tool for many branches of science researches and application systems.

An ultrafast pulse laser can generate pico- / femtosecond pulses with good quality, whose pulse duration, spectral bandwidth, peak power, repetition rate, etc, dependend on cavity design. Ultrasfast pulsed lasers can therefore be designed and utlized in various kinds of applications. Inside the laboratory, the main type of femtosecond pulse lasers is mode-locked solid state laser. For instance, mode-locked Ti:sapphire lasers, the most well-known and utilized ones, can provide the highest peak power and the shortest pulse duration at the same time as well as the stability which has been improved the last decade. However, outside the laboratory, the application of the solid state lasers is limited by their large size, frequent maintainance requirement, and high cost.

As comparison, mode-locked fiber pulse lasers are much more compact, more robust and cheaper, which makes them potentially capable in real application outside the laboratory. And fiber lasers also have advantages on highly efficient heat disspation,flexible output direction,easiness to couple with optical device, and so on. Therefore, mode-locked fiber lasers are promising for a wide range of applications such as gas sensing, optical coherent tomography (OCT) [13],high resolution remote scanning, gas sensing, optical comb generation, microscopy, and so on.

Researchers usually have two types of method to build a mode-locked fiber laser.One is to introduce an electric-driven modulator into the laser system, therefore an external signal is applied to realize a sinusoidal optical loss modulation inside the resonance cavity. This method is called active mode-locking, which will be introduced in section 3.2. Another method is to, contrast to the "active" mode-locking, passively self-modulate the intracavity loss with some special optical components. This method is called passive mode-locking. And the special optical components inside the cavity that provide a nonlinear optical anttenuation are called saturable absorbers (SA). Their optical absorbance decreases as the instantaneous input power increase. It is kind of like the light with higher power "saturate" the absorber and then suffers a lower absorbance, while the lower-power light will be absorbed more strongly. We will introduce passive mode-locking and saturable absorber in section 3.3 and section **??** respectively.

Saturable absorber is an essential optical component in passive mode-locked fiber laser system. It can be a semiconductor-based device (e.g. semiconductor saturable absorber mirror SESAM) [14], a fiber Kerr-effect-based device (e.g. nonlinear optical loop mirror NOLM, nonlinear polarization rotation NPR) [15, 16], or a natural nonlinear material (e.g. carbon nanotube, graphene) [17, 18].

1.2   Purpose of thesis

A drawback of the conventional passively mode-locked fiber lasers is that the repetition rate is relatively low, usually a few tens of megahertz. Passively mode-locked fiber lasers normally work in the fundamental mode. The repetition rate f_{rep} of the Fabry-Pérot type lasers in the fundamental mode is expressed as

$$f_{rep} = \frac{c}{2nL} \tag{1.1}$$

where L is the cavity length, n is the effective refractive index, and c is the velocity of light in vacuum. For a ring cavity fiber laser, f_{rep} is 2 times that of linear cavity with same cavity length. In order to raise the repetition rate up to the telecom date rate of a few gigahertz, the cavity length has to be shortened below 10 centimeters for Farby-Pérot laser's case. Fiber lasers with such a short cavity length require highly doped gain fiber, and a compact saturable absorber with low insertion loss. Here, carbon nanotube (CNT) is expected to meet the saturable absorber demanding while it offers several key advantages in ultrafast optics, such as hundreds-femtosecond level recovery time, compact size, low background loss, polarization independency, and the ability to operate both in transmission, reflection, and bidirection modes. The previous research has demonstrated 5-GHz-repetition-rate fiber laser [19], and then up to 20 GHz [20], using customized ultrahighly-Ytterbium:Erbium-co-doped fiber and CNT-SA. And for these short cavity lasers, no dispersion management is necessary because the short cavity only brings negligible dispersion so that saturable absorber can reshape pulses before dispersion effect is accumulated [19].

However, these short-cavity lasers operate in soliton mode-locking state. Here comes one problem that these lasers are unable to generate pulses with high pulse energy, because soliton pulses will be multipled, that is, the output will be unstable when further increased peak power induces more nonlinearity effect into the fiber cavity. To obtain high power pulses, one way is to mode-lock the resonator in the dissipative-soliton state, where the cavity has a net cavity dispersion at large normal dispersion region. But in Giga-Hertz-repetition-rate region, dissipative soliton is difficult to achieve because the cavity is too short to introduce intracavity filter components or effect. Therefore we consider stretched pulse, which can also generate high power pulse. So in this thesis, we try to use single-mode fiber to mode-lock the short-cavity fiber laser in streched-pulse state, that is, do dispersion management in short-cavity fiber laser.

During the experiment, another problem came out is that if we use commercially available Erbium doped fiber (EDF) to build the short laser cavity, higher pump power is required

to start CW lasing as well as mode-locking because the net gain will be quite low. And in Fabry-Pérot laser cavity, saturable absorber will be inevitably hit by the signal light and pump light simultaneously. The higher pump power will exceed the optical damage threshold of CNT before mode-locking starting. Then the CNT will be damaged and lose its optical non-linearity, no more supporting mode-locking the signal light. Our another purpose is to find and evaluate a substitute of CNT as saturable absorber which can tolerant high optical power circumstance. The material we investigate in this thesis is carbon nanotube @ boron nitride nanotube (CNT@BNNT). We will measure the optical nonlinearity of CNT@BNNT, and do comparision between it and CNT on optical damage threshold.

1.3   Organization of thesis

The organization of thesis is as follows: Chapter 2 introduces the propagation of the pulse inside optical fibers. Chapter 3 introduces the fundamentals of mode-locked fiber lasers. In Chapter4, we will introduce carbon nanotube (CNT) applied in ultrafast optics. And in Chapter 5, we will introduce and evaluate the newly-developed 1 dimensional material, carbon nanotube @ boron nitride nanotube (CNT@BNNT). In Chapter 6, dispersion managed short-cavity fiber lasers will be demonstrated.Finally, Chapter 7 makes the conclusion with an overview and some consideration of future work.

Chapter 2

Pulse Propagation in Fibers

Optical fibers, as light propagating media, shows some innegligible influencial factors when optical pulses propagating through. Under the influence of loss, birefringence, dispersion, nonlinear effect and so on, optical pulses' propagation process is accompanied with time-domain waveform and wavelength spectrum variation. In this chapter, we are going to explain the polarization induced nonlinearity and basic equation that governs the propagation of optical pulses in single-mode fibers (SMF). Then further discussion will be done when more influencial factors, especially group velocity dispersion (GVD) and self phase modulation (SPM) effect.

2.1   Nonlinearity in Optical Fibers

The propagation of optical fields in fibers is most fundamentally governed by Maxwell's equations, just like all the other electromagnetic phenomena. The equations take the form

$$\nabla \times \mathbf{E} = -\frac{\partial \mathbf{B}}{\partial t} \tag{2.1}$$

$$\nabla \times \mathbf{H} = J + \frac{\partial \mathbf{D}}{\partial t} \tag{2.2}$$

$$\nabla \cdot \mathbf{D} = \rho_f \tag{2.3}$$

$$\nabla \cdot \mathbf{B} = 0 \tag{2.4}$$

where $\mathbf{E}, \mathbf{H}$ are electric and magnetic field vectors, respectively, and $\mathbf{D}$ and $\mathbf{B}$ are corresponding electric and magnetic flux densities. The current density vector $\mathbf{J}$ and the charge density ρ_f represent the sources for the electromagnetic field. In the absence of free charges in a medium such as optical fibers, $\mathbf{J} = 0$ and $\rho_f = 0$.

The flux densities **D** and **B** arise in response to the electric and magnetic fields **E** and **H** propagating inside the medium, and the relation between them is give by

$$\mathbf{D} = \epsilon_0 \mathbf{E} + \mathbf{P} \tag{2.5}$$

$$\mathbf{B} = \mu_0 \mathbf{H} + \mathbf{M} \tag{2.6}$$

where ϵ_0 is the vacuum permittivity, μ_0 is the vacuum permeability, and **P** and **M** are the induced electric and magnetic polarizations. For optical fibers, $\mathbf{M} = 0$ because of nonmagnetic properties.

Like any other electromagnetic propagatation medium, Maxwell's equations can be used to describe the wave equation that describes the optical propagation in optical fibers. The wave equation can be expressed by **E** and **P** only as below:

$$\nabla \times \nabla \times \mathbf{E} = -\frac{1}{c^2}\frac{\partial^2 \mathbf{E}}{\partial t^2} - \mu_0 \frac{\partial^2 \mathbf{P}}{\partial t^2} \tag{2.7}$$

where c is the speed of light in vacuum and the relation $\mu_0 \epsilon_0 = 1/c^2$ is used here.In order to complete the description, we need a relation between the induced polarization **P** and the electric filed **E**. In general, a quantum-mechanical approach is required when evaluate the **P**, in the case that the optical frequency is near a medium resonance. However, we can use a phenomenological relation between **E** and **P** which is far from medium resonance. The relation is obtained by

$$\mathbf{P} = \epsilon_0 \left(\chi^{(1)} \cdot \mathbf{E} + \chi^{(2)} : \mathbf{EE} + \chi^{(3)} \vdots \mathbf{EEE} \cdots \right) \tag{2.8}$$

This is because for optical fibers, the wavelength range of interest for the study of fiber nonlinear effects is 0.5 - 2 μm. $\chi^{(j)}$ ($j = 1, 2, \ldots$) is jth order susceptibility.

$\chi^{(1)}$ is the linear susceptibility that represents the domaint contribution to **P**. It can be expressed by the relations between refractive index $n(\omega)$ and the absorption coefficient $\alpha(\omega)$ as

$$n(\omega) = 1 + \frac{1}{2}\,\mathrm{Re}[\tilde{\chi}^{(1)}(\omega)] \tag{2.9}$$

$$\alpha(\omega) = \frac{\omega}{nc}\,\mathrm{Im}[\tilde{\chi}^{(1)}(\omega)] \tag{2.10}$$

where Re and Im stand for the real and imaginary parts, respectively.

The second-order susceptibility $\chi^{(2)}$ is responsible for such nonlinear phenomena as second-harmonic generation and sum-frequency generation. However, for silica glass where SiO_2 is inversion symmetric in modeclar level, $\chi^{(2)}$ vanishes, so that optical fiber usually shows no second-order nonlinearity. Nonetheless, the electric-quadrupole and magnetic-dipole moments can generate weak second-order nonlinear effects, and under certain conditions defects or color centers inside the fiber core can somewhat also contribute to secon-harmonic generation.

The lowest-order nonlinear effects in optical fibers originate from the third-order susceptibility $\chi^{(3)}$, which is responsible for phenomena such as third-harmonic generation, four-wave mixing, and nonlinear refraction. However, unless special efforts are done to achieve phase matching, the nonlinear processes which involve the generation of new frequencies, such as third-harmonic generation and four-wave mixing, are not efficient in optical fibers. Therefore, the most considered nonlinear effect in optical fibers originates from nonlinear refraction, a phenomenon referring that the refractive index has an intensity depedence. This means that the n of optical fibers can be changable, which can be expressed as

$$\tilde{n}(\omega, I) = n(\omega) + n_2 I = n + \overline{n}_2 |E|^2 \tag{2.11}$$

where $n(\omega)$ is the linear part, I is the optical intensity associated with the electromagnetic field E, and $\overline{n}_2$ is the nonlinear-index coefficient related to $\chi^{(3)}$ by the relation

$$\overline{n}_2 = \frac{3}{8n} \operatorname{Re}(\chi_{xxxx}^{(3)}) \tag{2.12}$$

where Re stands the real part and the optical field E is assumed to be linearly polarized so that only one component $\chi_{xxxx}^{(3)}$ of the fourth-rank tensor contributes to the refractive index. The tensorial nature of $\chi^{(3)}$ can affect the polarization properties of optical beams through nonlinear birefringence.

If we include the third-order nonlinear effects governed by $\chi^{(3)}$, the induced polarization consists of two parts,

$$\mathbf{P}(\mathbf{r}, t) = \mathbf{P}_{\mathrm{L}}(\mathbf{r}, t) + \mathbf{P}_{\mathrm{NL}}(\mathbf{r}, t) \tag{2.13}$$

where the linear part $\mathbf{P}_{\mathrm{L}}$ and the nonlinear part $\mathbf{P}_{\mathrm{NL}}$ are related to the electric field by the general relations

$$\mathbf{P}_{\mathrm{L}} = \epsilon_0 \int_{-\infty}^{t} \chi^{(1)}(t - t') \cdot \mathbf{E}(\mathbf{r}, t') dt' \tag{2.14}$$

$$\mathbf{P}_{\mathrm{NL}}(\mathbf{r},t) = \epsilon_0 \int_{-\infty}^{t} dt_1 \int_{-\infty}^{t} dt_2 \int_{-\infty}^{t} dt_3$$
$$\times \chi^{(3)}(t-t_1, t-t_2, t-t_3) \vdots \mathbf{E}(\mathbf{r},t_1)\mathbf{E}(\mathbf{r},t_2)\mathbf{E}(\mathbf{r},t_3) \tag{2.15}$$

These relations are valid in the electric-dipole approximation and assume that the medium response is local.

2.2   Nonlinear Pulse Propagation

The study of most nonlinear effects in optical fibers utilizes short pulses with widths ranging from ~10 ns to 10 fs. When pulses with such short widths propagate inside a fiber, both dispersive and nonlinear effects will influence their time-domain waveform and wavelength spectra. By using Eqs(2.7) and (2.13), we can get the starting wave equation in the form

$$\nabla^2 \mathbf{E} - \frac{1}{c^2}\frac{\partial^2 \mathbf{E}}{\partial t^2} = \mu_0 \frac{\partial^2}{\mathbf{P}_{\mathrm{L}}} \partial t^2 + \mu_0 \frac{\partial^2 \mathbf{P}_{\mathrm{NL}}}{\partial t^2} \tag{2.16}$$

After solving the equation with various approximations, we can obtain the pulse propagation equation in dispersive nonlinear optical fibers as

$$\frac{\partial A}{\partial z} + \beta_1 \frac{\partial A}{\partial t} + \frac{i\beta_2}{2}\frac{\partial^2 A}{\partial t^2} + \frac{\alpha}{2}A = i\gamma(\omega_0)|A|^2 A\left(|A|^2 A + \frac{i}{\omega_0}\frac{\partial}{\partial T}(|A|^2 A) - T_{\mathrm{R}}A\frac{\partial|A|^2}{\partial T}\right) \tag{2.17}$$

where A is a slowly varying function which represents the pulse amplitude,and T is measured in a frame of reference moving with the pulses at the group velocity v_g ($T = t - z/v_g$). $|A|^2$ represents the optical power. α is loss coefficient representing the fiber absorption. β_1 and β_2 are chromatic dispersion coefficient, which govern the group velocity v_g and group velocity dispersion (GVD), respectively. They are expressed as

$$\beta_1 = \frac{1}{v_g} = \frac{1}{c}(n + \omega\frac{dn}{d\omega}) \tag{2.18}$$

$$\beta_2 = \frac{1}{c}(2\frac{dn}{d\omega} + \omega\frac{d^2 n}{d\omega^2}) \tag{2.19}$$

And γ is nonlinear coefficient which governs the nonlinear effects of self-phase modulation (SPM). It can be expressed with effective mode area A_{eff} as

$$\gamma = \frac{\omega_0 n_2}{c A_{\text{eff}}} \tag{2.20}$$

Equation (2.17) describes the propagation of a picosecond optical pulse in single-mode fibers. For pulses of width $T_0 > 5$ ps, the parameter $(\omega_0 T_0)^{-1}$ and (T_R/T_0) become so small that the last two terms in Eq.(2.17) can be neglected. Then Eq.(2.17) can be reduced to the form

$$i\frac{\partial A}{\partial z} + \frac{i}{2}\alpha A - \frac{1}{2}\beta_2 \frac{\partial^2 A}{\partial T} + \gamma |A|^2 A = 0 \tag{2.21}$$

If assume the pulse propagating in SMF with negligible loss ($\alpha = 0$), we can get the nonlinear Schrödinger equation (NLSE). Moreover, by further expanding this correspondence, the Eq. (2.17) is often referred to as the generalized nonlinear Schrödinger equation. Eq. (2.21) appears in various situations in optics.

2.3   Group-Velocity Dispersion

Group-velocity dispersion (GVD) is the phenomenon in which a difference in the travelling speed (group velocity v_g) of light depends on the wavelength. The phenomenon where the long wavelength light travels faster and the short wavelength light travels slower is called normal dispersion. The contrast phenomena where the short wavelength light travels faster and the long wavelength light travels slower is called anomalous dispersion. This section will discuss the GVD effects on pulses.

In section 2.2 we foused on the nonlinear Schrödinger equation which describes the propagation of optical pulses inside SMF. For pulse width > 5 ps, we can use Eq. (2.21) in a rearranged form

$$i\frac{\partial A}{\partial Z} = -\frac{i\alpha}{2}A + \frac{\beta_2}{2}\frac{\partial^2 A}{\partial T^2} - \gamma |A|^2 A \tag{2.22}$$

The three terms on the right-hand side of Eq. (2.22) govern the effects of fiber losses, dispersion, and nonlinearity, respectively, on pulses propagating inside optical fibers. Depending on the initial width T_0 and the peak power P_0 of the incident pulse, either dispersive or nonlinear effects may dominate the influence along the fiber travelling.

Here we first introduce two useful length scales, known as the dispersion length L_D and the nonlinear lenth L_{NL}. The two parameters are expressed as

$$L_D = \frac{T_0^2}{|\beta_2|}, \qquad L_{NL} = \frac{1}{\gamma P_0} \tag{2.23}$$

respectively. Depending on the relative magnitudes of L_D, L_{NL} and the fiber length L, pulses can evolve quite differently. L_D and L_{NL} provide the length scale over which dispersive or nonlinear effects become important for pulse evaluation. In this section, we focus on the effect of dispersion, so we assume that $L_D/L_{NL} \ll 1$. The assumption means that the dispersive effect in optical fibers is so stronger than the nonlinear effect that it takes much shorter pulse-propagation distance for dispersive effect to accumulate than nonlinear effect does.

Then, let us define a time scale normalized to the input pulse width T_0 and a normalized amplitude U, respectively, as

$$\tau = \frac{T}{T_0} = \frac{t - z/v_g}{T_0} \tag{2.24}$$

$$A(z, \tau) = \sqrt{P_0} exp(-\alpha z/2) U(z, \tau) \tag{2.25}$$

where P_0 is the peak power of the incident pulse. The exponential factor in Eq. (2.25) accounts for fiber losses. By using Eqs (2.22)-(2.25), $U(z, \tau)$ is calculated to satisfy

$$i\frac{\partial U}{\partial z} = \frac{sgn(\beta_2)}{2L_D} \frac{\partial U}{\partial \tau^2} - \frac{exp(-\alpha z)}{L_{NL}} |U|^2 U \tag{2.26}$$

where $sgn(\beta_2) = \pm 1$ depending on the sign of the GVD parameter β_2. In this section's discussion, the nonlinear effect is negligible, and the normalized propagation equation can be expressed as

$$i\frac{\partial U}{\partial z} = \frac{\beta_2}{2} \frac{\partial^2 U}{\partial T^2} \tag{2.27}$$

This equation can be solved by using Fourier-transform method. If define $\tilde{U}(z, \omega)$ as the Fourier transform of $U(z, T)$, the general solution is given by

$$U(z, T) = \frac{1}{2\pi} \int_{-\infty}^{+\infty} \tilde{U}(0, \omega) exp\left(\frac{i}{2}\beta_2\omega^2 z - i\omega T\right) d\omega \tag{2.28}$$

where $\tilde{U}(o, \omega)$ is the Fourier transform of the incident field at $z = 0$ and is obtained by

$$\tilde{U}(0, \omega) = \int_{-\infty}^{+\infty} U(0, T) exp(i\omega T) dT \tag{2.29}$$

Equations (2.28) and (2.29) can be used for arbitrarily shaped input pulses.

As a simple example, consider the case of a Gaussian pulse $U(0, T) = exp(-T^2/2T_0^2)$. T_0 is the half-width (at 1/e-intensidy point),which can be replaces as T_{FWHM} in practice. The amplitude of the incident pulse at any point z along the fiber is given by

$$U(z,T) = \frac{T_0}{(T_0^2 - i\beta_2 z)^2} exp\left[-\frac{T^2}{2(T_0^2 - i\beta_2 z)}\right] \tag{2.30}$$

Thus, a Gaussian pulse maintains its shape on propagation but its width T_1 increases with z as

$$T_1(z) = T_0[1 + (z/L_D)^2]^{\frac{1}{2}} \tag{2.31}$$

If we write $U(z,T)$ in the form

$$U(z,T) = |U(z,T)|exp[i\phi(z,T)] \tag{2.32}$$

where

$$\phi(z,T) = -\frac{sgn(\beta_2)(zL_D)}{1 + (z/L_D} \frac{T^2}{2T_0^2} + \frac{1}{2}tan^{-1}\left(sgn(\beta_2)\frac{z}{L_D}\right) \tag{2.33}$$

The time dependence of $\phi(z,T)$ implies that the instantaneous frequency differs across the pulse from the central frequency ω_0. The difference $\delta\omega$ is given by

$$\delta\omega(T) = -\frac{\partial\phi}{\partial T} = \frac{sgn(\beta_2)(z/L_D)}{1 + (z/L_D^2)} \frac{T}{T_0^2} \tag{2.34}$$

Equation (2.34) shows that the frequency changes linearly across the pulse, which means that a fiber imoses linear frequency chirp on the pulse. The chirp $\delta\omega$ depends on the sign of β_2. In the normal-dispersion regime ($\beta - 2 > 0$), $\delta\beta$ is negative at the leading edge ($T < 0$) and increased linearly across the pulse. The opposite occurs in the anomalous-dispersion regime ($\beta_2 < 0$).

Then we consider the case of a linearly chirped Gaussian pulse whose incident field can be written as

$$U(0,T) = exp\left(-\frac{(1+iC)}{2}\frac{T^2}{T_0^2}\right) \tag{2.35}$$

where C is a chirp parameter. The amplitude of the incident pulse at any point z along the fiber is and the pulse width are given by

$$U(z,T) = \frac{T_0}{[T_0^2 - i\beta_2 z(i + iC)]^{\frac{1}{2}}} exp\left(-\frac{(1 + iC)T^2}{2[T_0^2 - i\beta_2 z(1 + iC)]}\right) \qquad (2.36)$$

$$\frac{T_1}{T_0} = \left[\left(1 + \frac{C\beta_2 z}{T_0^2}\right)^2 + \left(\frac{\beta_2 z}{T_0^2}\right)^2\right]^{\frac{1}{2}} \qquad (2.37)$$

From these equations we can know that chirped pulses may broaden or compress depending on whether β_2 and C have the same or opposite signs. When $\beta_2 C > 0$, a chirped Gaussian pulse broadens monotonically at a rate faster than that that of the unchirped pulse. The reason is related to the fact that the dispersion-induced chirp adds to the input chirp because the two contributions have the same sign. The situation changes dramatically for $\beta_2 C < 0$. The chirped pulse narrows in a regime where z is small. That is, the chirped pulse width can be compressed by passing the dispersive medium with the opposite sign. The minimum point of the pulse width is where the two chirps with opposite signs just cancel each other.

2.4   Self-Phase Modulation

High optical intensity in a medium (e.g. optical fiber) will cause a change of refractive index. This phenomenon is called optical Kerr effect. Self-phase modulation (SPM) is one of the nonlinear effect originates from Kerr effect, which leads to spectral broadeing of optical pulses.

In section 2.3 we discussed how group velocity dispersion effect influences the pulse propagation inside optical fibers with negligible nonlinear effect. Another simplification of Eq. (2.21) occurs under the assumption that the effect of GVD on SPM is negligible so that the β_2 term can be set to zero. The length scale L_D and L_{NL} are inroduced in section 2.3. In general, the pulse width and the peak power should be such that $L_D \gg L > L_{NL}$ for a fiber length L. In terms of the normalized amplitude $U(z,T)$ defined in Eq. (2.25), the pulse propagation Eq. (2.26) in the limit $|beta_2$ becomes

$$\frac{\partial U}{\partial z} = \frac{ie^{-\alpha z}}{L_{NL}}|U|^2 U \qquad (2.38)$$

where α accounts for fiber losses. The equation can be solved directly as

$$U(L, T) = U(0, T) exp[i\phi_{NL}(L, T)] \tag{2.39}$$

$$\phi_{NL}(L, T) = |U(0, T)|^2 (L_{eff}/L_{NL}) \tag{2.40}$$

$$L_{eff} = [1 - exp(-\alpha L)]/\alpha \tag{2.41}$$

Equation (2.40) shows that SPM induces rise to an intensity-dependent phase shift ($L_{NL} = (\gamma P_0)^{-1}$) but the pulse shape remains unaffected. The nonlinear phase shift ϕ_{NL} in Eq. (2.41) increases with fiber length L. The quantity L_{eff} plays the role of an effective length that is smaller than L because of fiber lossed. In the absence of fiber losses, $\alpha = 0$, and $L_{eff} = L$. The maximum phase shift occurs at the pulse center located at $T = 0$. With U normalized such that $|U(0, 0)| = 1$, it is given by

$$\phi_m ax = L_{eff}/L_{NL} = \gamma P_0 L_{eff} \tag{2.42}$$

Spectral broadening induced by SPM is a direct consequence of the time dependence of ϕ_{NL}. A temporally varying phase implies that the instantaneous optical frequency differs across the total pulse from its central value ω_0. The difference $\delta\omega$ is given by

$$\delta\omega(T) = -\frac{\partial\phi_{NL}}{\partial T} = -\left(\frac{L_{eff}}{L_{NL}}\right)\frac{\partial}{\partial T}|U(0, T)|^2 \tag{2.43}$$

The time dependence of $\delta\omega$ is referred to as frequency chirping. The chirp induced by SPM increases in magnitude with the propagated distance. That is, new frequency components are generated continuously as the pulse propagates along the fiber. These SPM-generated frequency components broaden the spectrum over its initial width at $z = 0$ for initially unchirped pulses.

The qualitative features of frequency chirp depend on the pulse shape. Consider the case of a super-Gaussian pulse with the incident fielf $U(0, T)$ given by

$$U(0, T) = exp\left[-\frac{1 + iC}{2}\left(\frac{T}{T_0}\right)^{2m}\right] \tag{2.44}$$

The SPM-induced chirp $\delta\omega(T)$ for such a pulse is

$$\delta\omega(T) = \frac{2m}{T_0}\frac{L_{eff}}{L_{NL}}\left(\frac{T}{T_0}\right)^{2m-1} exp\left[-\left(\frac{T}{T_0}\right)^{2m}\right] \tag{2.45}$$

$m = 1$ is for Gaussian pulse. For larger values of m, the incident pulse becomes nearly rectangular with increasingly steeper leading and trailing edges. The Eq. (2.45) shows some

features. First, $\delta\omega$ is negative near the leading edge (a red shift) and becomes positive near the trailing edge (a blue edge) of the pulse. Second, the chirp is linear and positive (up-chirp) over a large central region of the Gaussian pulse. Third, the chirp is considerably larger for pulses with steeper leading and trailing edges. Fourth, super-Gaussian pulses behave differently than Gaussian pulses because the chirp occurs only near pulse edges.

Section 2.3 and 2.4 solved pulse propagation equation under the assumption of negligible nonlinear or dispersion effect, respectively. When the pulses are relatively long ($T_0 < 50$ ps), the dispersion length L_D is much larger compared with both the fiber length L and the nonlinear length L_{NL}. As pulses become shorter and the dispersion length becomes comparable to the fiber length, it becomes necessary to consider the combined effects of GVD and SPM. New qualitative features arise from an interplay with GVD and SPM. In the anomalous-dispersion regime of an optical fiber, the two effects can cooperate in such a way that the pulse propagates as an optical soliton. The temporal chirp and spectral chirp exactly cancel each other resulting a preservation of temporal and spectral shape of pulses even over long propagation distance. In the normal-dispersion regime, the two kinds of chirp are combined and can be used for pulse compression.

Chapter 3

Mode-locked Fiber Laser

3.1 Mode-locking

In a laser cavity, light frequencies which circulate inside the resonator and have more gain than losses are called longitudinal modes. Lasers operate simultaneously in a large number of longitudinal modes locating within the gain bandwidth. These londitudinal modes are spaced in an equal interval. This intercal is called free spectral range (FSR), which is give by

$$\Delta\nu = c/L_{\text{cavity}} \tag{3.1}$$

where L_{cavity} is the optical length of one round trip in the laser cavity. And this equation is as same as Eq. (1.1), that is, FSR is equal to laser's fundamental repetition rate. Longitudinal modes can be considered as an assembly of independent oscillators. We can write down the total optical field as an sum of all the individual londitudinal modes like

$$E(t) = \sum_{m=-M}^{M} E_m exp(i\phi_m - i\omega_m t) \tag{3.2}$$

where E_m, ϕ_m and ω_m are the amplitude, phase and frequency of the m mode. The total number of longitudinal modes is $N = 2M + 1$.

When these londitudinal modes oscillate independently on each other, the interference terms in the total intensity $|E(t)|^2$ disappear and the total intensity shows a time independence. The laser is in continuous wave state.

However, if the phases of various longitudinal modes are fixed so that the phase difference between any two neighboring modes is locked to a constant value, which means $\phi_m - \phi_{m-1} = \Delta\phi$, or $\phi_m = m\Delta\phi + \phi_0$. As $\omega_m = \omega_0 + 2\pi m\Delta\nu$, and for simplicity, if we
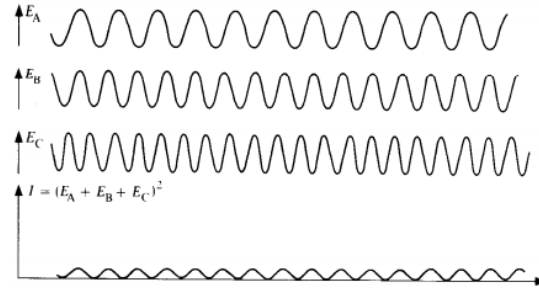
Fig. 3.1 Output signal from laser with longitudinal modes oscillating independently. [21]
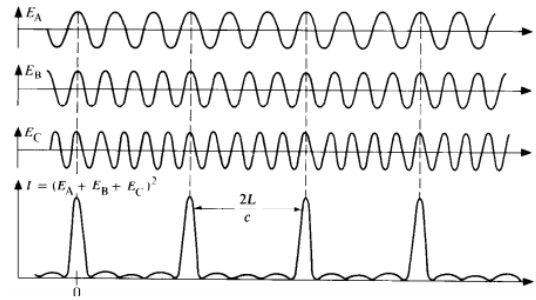
Fig. 3.2 mode-locked laser output signal. [21]

assume all modes have the same amplitude, the power of the assembled longitudinal modes can be calculated as

$$|E(t)|^2 = \frac{\sin^2(N\pi\Delta vt + \phi/2)}{\sin^2(\pi\Delta vt + \phi/2)} E_0^2 \qquad (3.3)$$

Figure **??** and 3.2 show a three-modes laser oscillating state without and with mode-locking mechanism, respectively. We can clearly see that, with mode-locking mechanism, an output of pulse train with a repetition rate of Δv is obtained. The phenomenon can be explained simply as, inside the resonator there is a single pulse circulating aroung a trip period of $\tau_r = 1/\Delta v$, and every time the pulse hits the output coupler it will release a copy outward with part of the energy. From Eq. (3.3), the pulse width is calculated as $\tau_p = [(2M + 1)\Delta v]^{-1}$, where $(2M + 1)\Delta v$ represents the bandwidth of $(2M + 1)$ londitudinal modes. It can be considered as mode-locked lasers with larger spectrum bandwidth generate pulses with shorter pulse width. Meanwhile, pulse's intensity is proportional to M^2. For real laser mode-locking, the number of longitudinal modes are usually more than 1000. Therefore, pulses with ultrashort pulse width and ultrahigh peak power can be obtained with mode-locking mechanism.

The main methods to realized mode-locking are active mode-locking and passive mode-locking, and the one hybrid from these two methods.

3.2   Active Mode-locking

Active mode-locking refers to the method that modulates the amplitude or frequency (or phase) of the optical field inside the cavity at a modulation frequency f_m equal to the longitudinal mode space $\Delta \nu$. According to the modulated factory the method can be called AM (amplitude modulation) or FM (frequency modulation) mode-locking. In either AM or FM mode-locking, modulation sidebands appear beside every longitudinal mode spaced at a modulation frequency f_m. If $F_m = \Delta \nu$, the sidebands overlap adjacent modes and the phase imformation of one mode is passed to the next mode through the modulation sideband. Strictly speaking, the distance between each longitudinal mode is not equal to $\Delta \nu$ due to the influence such as the dispersion effect from the optical medium, the sidebands are located in the immediate vicinity of the adjacent mode. This sideband acts as an injection signal for the adjacent mode and serves to pull the oscillation frequency of the adjacent mode to $\nu_m + f_m$. By this overlap, overall phase fix occurs and mode-locking is realized.

We can also comprehend the pulse formation process on time-domain. Fig. 3.3 shows the case of AM mode-locking. The resonator losses are modulated at the frequency of $\Delta \nu$. Since the light inside the laser is strong when the losses are minimal, the electric field inside the resonator, and consequently the laser output, is modulated at the same frequency. This small difference in intensity accumulated as light circulatting aroung the resonator, which leads to a mode-locked pulse train output when the laser comes to a steady state. In other words, the loss-modulated resonator favors pulse oscillation rather than CW oscillation. This is because the intracavity light intensity is present only when the loss is low. This lower the threshold for pulse oscillation and suppress the existence of CW oscillation. As a result, the laser emits a pulse train rather than a CW. FM mode-locking works the same way.
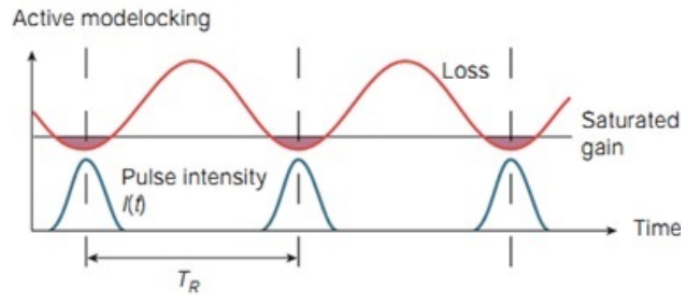

Fig. 3.3 Active mode-locking mechanism in time-domain

The advantages of active mode-locking are that it is easy to achieve high repetition-rate mode-locking and is easy to synchronize with other lasers for modulation. The disadvantage is that the pulse duration obtained is relatively larger than that from a passive mode-locked laser. And a modulator required inside active mode-locked laser's cavity is usually difficult to compact, which makes it difficult to miniaturize the laser.

3.3   Passive Mode-locking

Passive mode-locking, different from active mode-locking, does not require an intra-cavity modulator driven by external signal. It is a method which utilizes nonlinear effect to generate ultrashort pulses. Instead of an active modulator, an intensity dependent optical absorber is incorporated into the resonator to help realize mode-locking.

A saturable absorber is an element having the property that the light absorbance decreases as the intensity of incident light increases. In the following, we consider a steady state, where a short pulse is already circulating in the laser resonator. For simpilicity, it is assumed that there is only one circulating pulse and a fast saturable absorber is used. Every time the pulse hits the saturable absorber, it saturates the absorption, thus temporarily reducing the losses. In the steady state, the laser gain can be saturated to a level which is just sufficient for compensating the losses for the circulating pulses, whereas any light with lower intensity such as background continuous light or noise spikes will experience losses which are higher than the gain,since the absorber cannot be saturated by this light, as shown in Fig. 3.4a. The saturable absorber can thus suppress any additional weaker pulses as well as continuous background light every round trip. Also, it constantly sharpens particularly the leading wing of the circulating pulse while the trailing tail may also be sharpened if the saturable absorber has a sufficiently short recovery time (fast enough). The circulating pulse thus experiences a width suppression accumulation during the intracavity circulating before the steady state is achieved. And in the steady state, saturable absorber can help balance some other effects (e.g. dispersion) which tend to length the pulse, see in Fig. 3.4b.

In the precious statement we assumed a short pulse has already existed inside the resonator to explain how saturable absorber works in passive mode-locking. However there is a much more complicated passive mode-locking process. Fluctuations of the incident spontaneous emission light are magnified by saturable absorber while circulating around the resonator, and the fluctuations become pulse which is strong enough to saturate the saturable absorber. This pulse continues to shorten until its spectal width exceeds the gain width. For fiber lasers, group-velocity dispersion and self-phase modulation also play an important role in mode-locked pulse generation. Therefore, the passive mode-locked fiber laser theory is
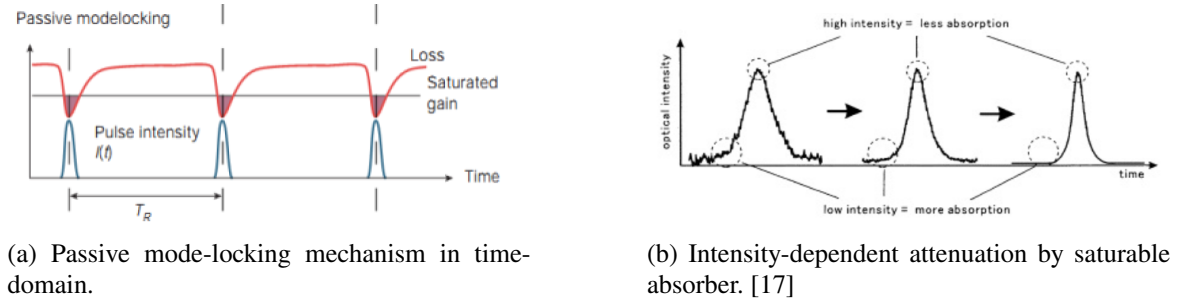
(a) Passive mode-locking mechanism in time-domain.

(b) Intensity-dependent attenuation by saturable absorber. [17]

Fig. 3.4 passive mode-locking

based on the nonlinear Shrödinger equation and two extra elements: a finite gain bandwidth of the gain medium and an intensity-dependent loss from saturable absorber. As a result, a passive mode-locked fiber laser outputs chirp-soliton pulses, whose amplitude $u_s(\tau)$ is

$$u_s(\tau) = N_s[sech(p\tau)]^{l+iq} \tag{3.4}$$

where N_s, p, q are pulse parameters related with soliton pulse width T_s, inverse of gain spectral width T_2, peak power P_s and frequence chirp $\delta\omega$ by

$$T_s = \frac{T_2}{p} \tag{3.5}$$

$$P_s = |\beta_2|\frac{N_s^2}{\gamma T_2^2} \tag{3.6}$$

$$\delta\omega = \frac{q\tanh(pr)}{T_s} \tag{3.7}$$

Compared to active mode-locking, the technique of passive mode-locking allows the generation of much shorter pulses, essentially because a saturable absorber can modulate the resonator losses much faster than any electronic modulator. And saturable absorbers are usually easy to compact with fiber lasers. As disadvantages, it is quite difficult for passive mode-locking to achieve high-repetition-rate mode-locking.

To build a passive mode-locked laser, many kinds of saturable absorbers, natural or artificial, can be chosen according to design requirements. For example, nano cabon materials like carbon nanotube (CNT) [17]and graphene [18], fiber devices based on nonlinearity of optical fibers such as nonlinear (amplified) loop mirror (NOLM, NALM) [22] and nonlinear polarization rotation (NPR) [23], semiconductor saturable absorber mirror (SESAM) [14]. Recent years two dimensional materials like WTe$_2$ [24] and MXene [25] are used to enrich

the choice of saturable absorbers. In this thesis, we mainly investigate CNT and its derivative CNT@BNNT, which will be introduced in section 3.4 and Chapter 4, respectively.

3.4   Carbon Nanotube

Single-walled CNT is a rolled single-layer graphene, whose typical diamater is ~1 nm and length is ~1 μm, thus we call it a long 1-D material [26, 27] [Fig. 3.5a]. The CNT structure, which determines electronic band structures, is determined by how the single-layer graphene is rolled, and is expressed by a single parameter, chirality $\mathbf{C}_h$. For chirality also determines the tube diameter, we usually use tube diameter to indicate CNT's electronic properties. [28]. In the CNT having a chiral vector $\mathbf{C}_h$, the wave vector $\mathbf{k}$ has to satisfy the periodic boundry condition $\mathbf{C}_h \cdot \mathbf{k} = 2q\pi$, where q is an integer. As a result, electronic band structure of a specific CNT is given by a superposition of cuts of the graphene-type electronic energy bands along the corresponding allowed $\mathbf{k}$ lines (cutting lines). This is called "Zone-folding approximation", which ignores the curvature effects in CNTs. In case one of the cuts contains the Dirac (K) point (the point where the valence band and conduction band meet taking the shape of the upper and lower halves of a conical surface), the CNT is metalic [Fig.3.6(a)]. Otherwise, it is semiconducting and has bandgap [Fig.3.6(b)]. It is shown that $n - m = 3k$ (k: integer) for metalic CNTs, and $n - m \neq 3k$ for the semiconducting CNTs. Fig. 3.6(c) and (d) show examples of the calculated density of states of a metallic (9,0) CNT and a semiconducting (10,0) CNT [29]. Optical transitions can occur between the bandgaps $v_1 - c_1$, $v_2 - c_2$,..., labeled as E_{11}, E_{22},...In semiconductiong CNTs, the first bandgap energy E_{11} is inversely propotional to the tube diameter d, as

$$E_{11} = 2\gamma_0 a_{C-C}/d \tag{3.8}$$

Corresponding to the optical bandgaps, the semiconducting CNTs have peak absorption wavelength. Fig. 3.5b shows a typical transmission spectrum of a CNT sample. Typical CNT diameter in a sample is 0.7-1.5 nm, whose bandgap energy of 1.2-0.6 eV calculated from Eq.(3.8), corresponding to the optical wavelength of 1-2 μm. In current fabrication methods, selective growth of single chirality of CNT is not available yet, so that a CNT sample is always a mixture of several or many kinds of semiconducting and metallic CNTs. Chirality distribution is determined by the fabrication method, and mean tube diameter is controlled somehow by fabrication condition. Moreover, although the technique to fabricate aligned CNT sample, we can still use the randomly oriented CNT sample to eliminate polarization dependence.
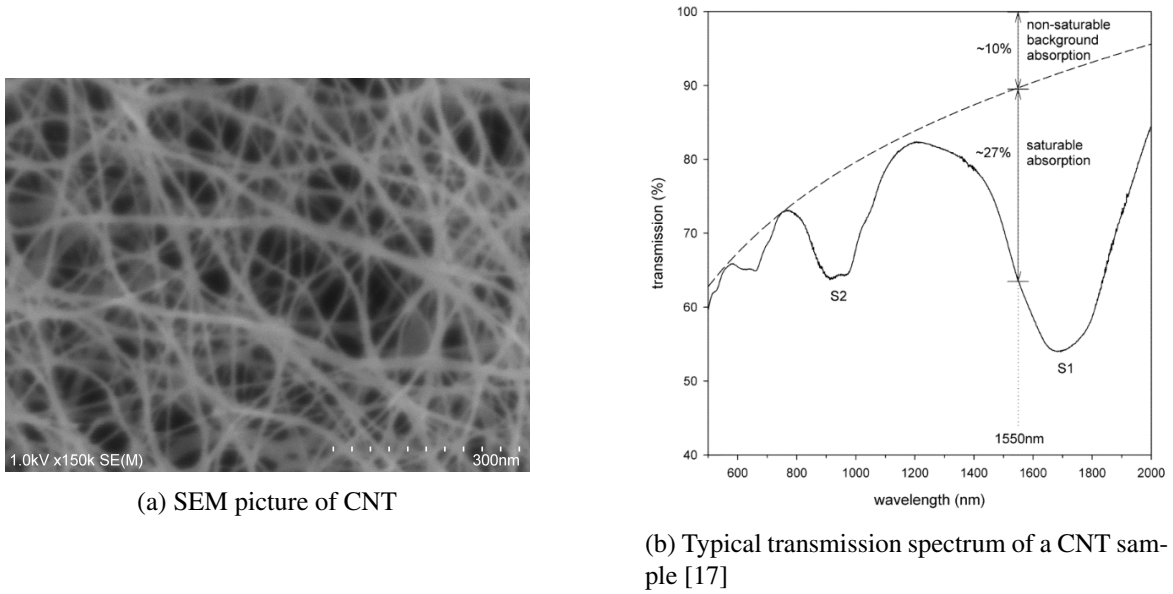
(a) SEM picture of CNT

(b) Typical transmission spectrum of a CNT sample [17]

Fig. 3.5 Typical CNT sample

CNT has inherently fast recovery time, which makes it more competive. In case of semiconducting CNTs, the recovery time of E_{11} transition is an order of 1 ps, and that of E_{22} transition is at an even faster order of 100 fs, as shown in Fig. 3.7 [30]. The opening of the band gap in semiconducting CNTs determines the saturable absorption dynamics over the whole visible and nearinfrared spectrum. Meanwhile, it is believed that tube-tube interaction, that is, tunneling of the free carriers from semiconducting into metallic CNTs assistances the transmition process to be fast. This idea is supported by the experimental fact that the isolated semiconducting CNTs have slower saturable absoprtion of ∼30 ps [31].
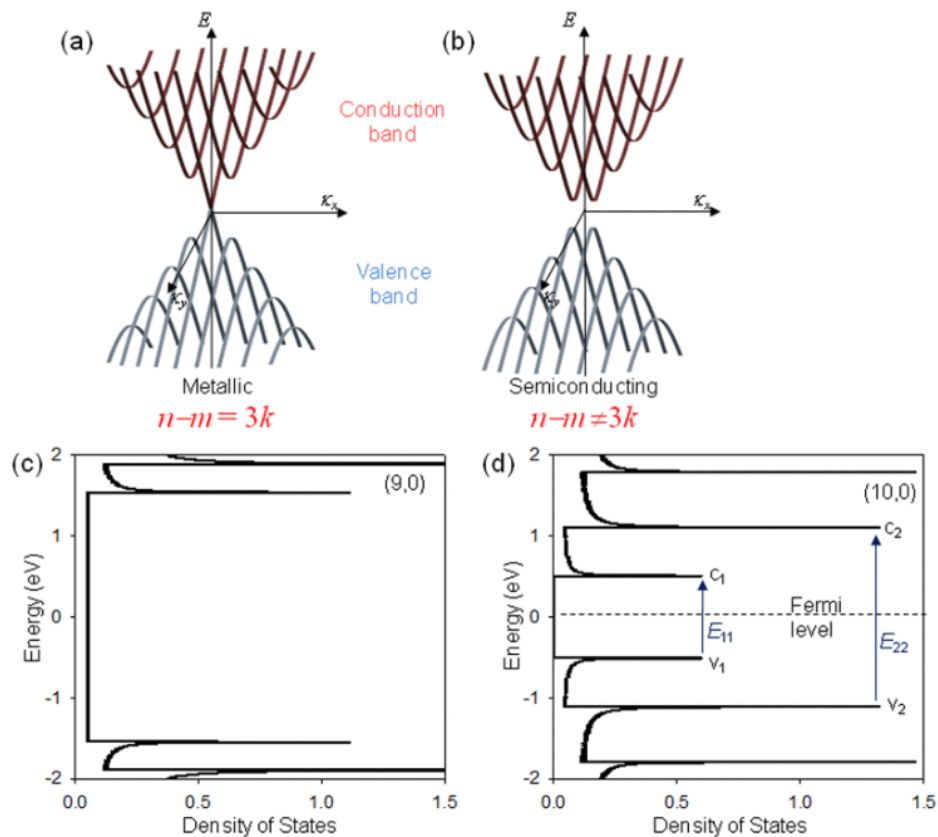
Fig. 3.6 Band structures and density of states of (a), (c) metallic CNT, and (b), (d) semiconducting CNT. [26]
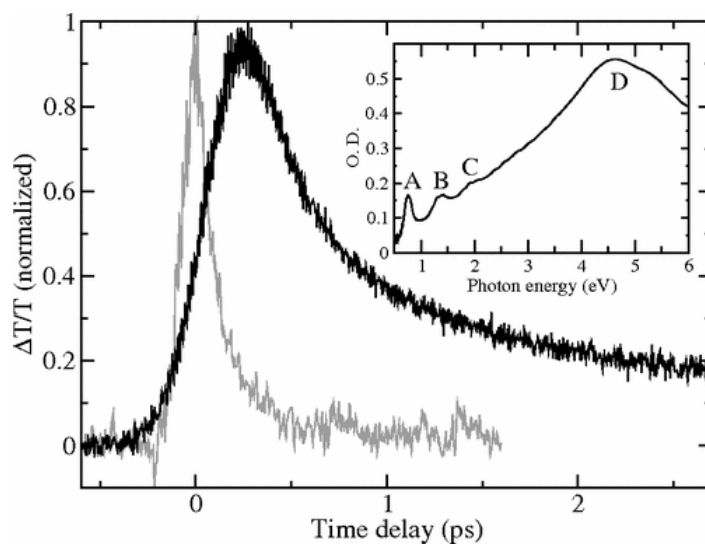
Fig. 3.7 Transmittivity transients for semiconducting CNTs [30]

Chapter 4

CNT@BNNT Saturable Abosrber

4.1 Low Optical Power Durabilty

In section 3.4 we explained CNT as saturbale absorber in detail. We choose CNT as saturable absorber in this thesis fot reasons like compativity, fast recovery time and so on. However in the actual experiment, we met the problem that when CNT was hit by light, signal or pump light, with high power exceeding tens of mW, CNT was burnt out by the accumulated heat and the following oxidation [32]. That is, under high power situation, CNT will lose its optical nonlinearity or even degrade to optical dust, which will futher damage optical components like fiber ferrules and fiber-type mirrors. Fig. 4.1 shows a burn mark appeared on the center of a fiber ferrule. We sprayed CNT onto this fiber ferrule, then coupled this CNT-sprayed ferrule into laser cavity trying to mode-lock the laser. As we used a low-gain cavity, relatively high pump power seemed to be required. But after we increased the pump power to around 100 mW, we found the CNT on the ferrule was burnt out, so well as the fiber ferrule. The CNT cannot be used and the ferrule should be repolished.

This experimental trouble comes from CNT's well-known drawback, low thermal damage threshold. In optical application, CNT's low damage threshold will not only suppress the optical power upper limit inside the laser cavity, but somehow influence the design of laser cavity setup. This problem is particularly important in short-cavity mode-locked fiber lasers [33, 34].Therefore, there is the need for SA substitution of CNT with higher damage threshold. In this chapter, we will introduce a newly developed nanotubular material, carbon nanotube @ boron nitride nanotube (SWCNT@BNNT), as a saturable absorber synthesized from CNT. Then its saturable absorption and optical damage threshold will be investigated and compared to those of CNT.
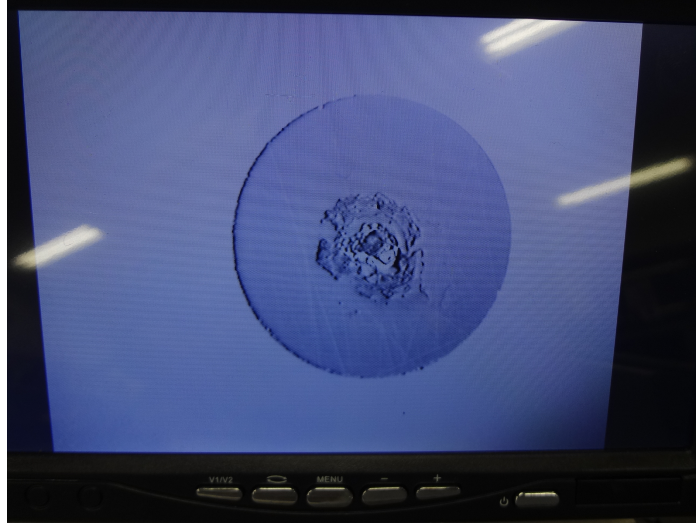
Fig. 4.1 A burn mark caused by burnt CNT on fiber's ferrule.

4.2 CNT With BNNT

With the further research development and application need coming out, researchers in various fields try to isolate and reassemble the existing tubular/planar nanomaterials into heterostructures. Every layer is piled in a precisely chosen sequence. These artificial novel function-designed nanomaterials are called van der Waals (vdW) heterostructures [35, 36]. This concept was firstly proposed to general name these 2D reassembled materials, then it was extended to 1D materials like carbon nanotube (CNT), Boron Nitride nanotube (BNNT), and so on. See Fig. 4.2. [37] Researchers design and synthesize these kinds of hybrid materials to achieve desired electrical / chemical / mechanical properties, like bandgap adjustment, shell protection and so on [38]. This technique is therefore a promising approach to solve the problem mentioned above. The target here is to improve CNT's optical damage threshold without influencing the band structure area where saturable absorption occurs. Under this context, BNNTs are chosen to team up with CNTs to achieve the goals. And we name this heterostructure concentric multi-walled nanotubes consisting of inner carbon nanotube and external boron nitride nanotubes as CNT@BNNTs.

4.2.1 Electronic Band Structures

Under local density approximation and quasi-partical calculatons, BNNTs are semiconducting with a bandgap of roughly 5.5 eV when BNNTs were firstly proposed [39]. Although the bandgaps may vary slightly with the chiriality, BNNT's bandgap area is generally larger than that of CNT ($\sim$ 1 eV) where saturable absorption occurs. See Fig. 4.3. Moreover, ac-

(a) Lego blocks showing one dimensional vdW heterostructure.

(b) Atomic model of a single-walled CNT wrapped with two layers of BNNT.
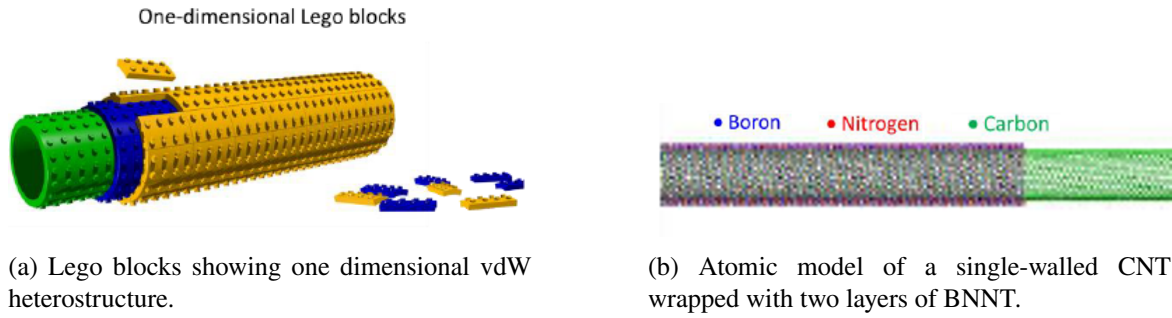
Fig. 4.2 Models of CNT@BNNT [37]

cording to the first-principle calculations of the electronic structure of the concentric tubular materials, the original hyperconjugated network of the inner SWCNT electronic states is barely affected by the outer BN shell [38]. Neither extra conduction band or valence band will be introduced into CNTs' band gap, nor will bands hybridization happen after wrapping BNNT around CNT. See Fig. 4.4. Although the CNT used in band structure calculation of Fig 4.4 is metallic, we can still make resonable assumption that the caculation result applies to semiconducting CNT, since BN-wrapping dose not influence the chirality distribution of inner CNT, which will be further confirmed in section 4.7.

These caculations supports the idea that in vis-NIR wavelength region (photon energy less than BNNT bandgap energy), the optical phenomena such as saturable absorption can still happen after CNT wearing a BN armor.
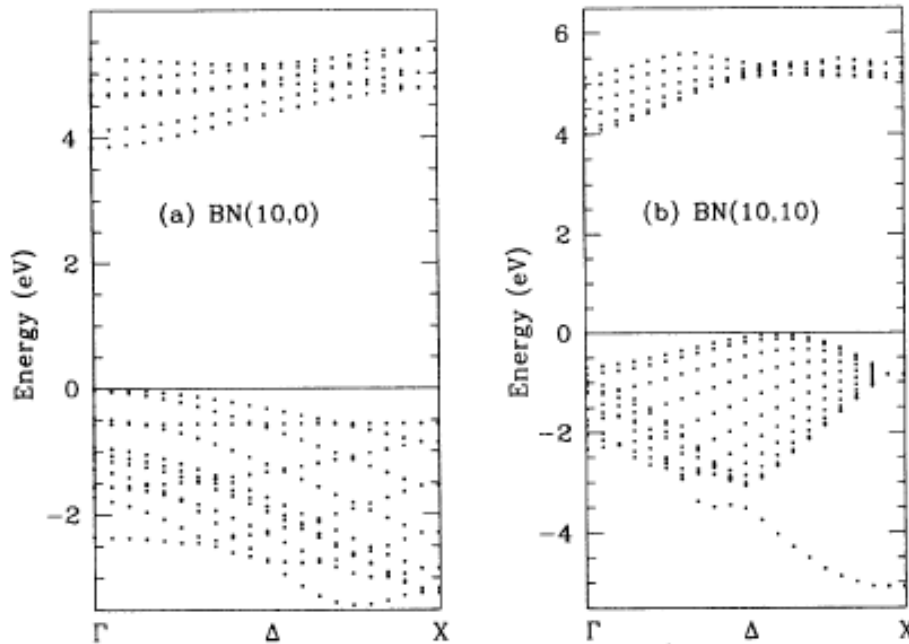
Fig. 4.3 Caculated bandstructure of two kinds of BNNT with different chirality. [39]
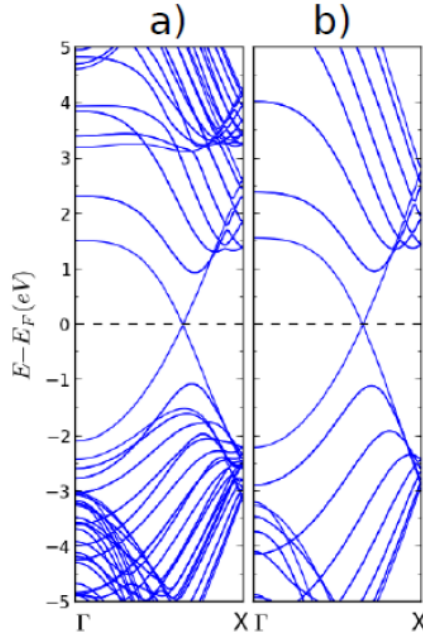
Fig. 4.4 Caculated band structures of (a) a double-walled hybrid nanotube formed by an inner (7,7) CNT concentric to a (12,12) BNNT and (b) a (7,7) CNT. [38]

4.2.2   Thermal Stability

In air, CNT will be burned at a temperature of 450°C. As a protective shell of CNTs, BNNTs are resistive to oxidation up to around 900°C, which is much higher than that of CNT. On the other hand, BNNT is a comparable or even better thermal conductor, compared to CNT [40], which indicates that there will not be more heat accumulating on BNNT than on isolated CNT. These makes BNNTs ideal candidates for operating under high thermal and optical-power conditions, as well as an overall armor against oxygen for CNT, as Fig. 4.5 shows. As a result, the synthesized CNT@BNNT can be resistive to heating in air up to 700°C. Meanwhile, BNNT's thermal stability and chemical inertness guarantee that the synthesis of CNT@BNNT can be processed smoothly.

4.3   Synthesis of CNT@BNNT

In this section, we will demonstrate the synthesis method of CNT@BNNT. The material is fabricated by Maruyama Lab, university of Tokyo.

Figure 4.6 shows a standard chemical vapor deposition (CVD) system which is used for BN coating. Firstly, a piece of single-walled CNT film has been prepared as template before
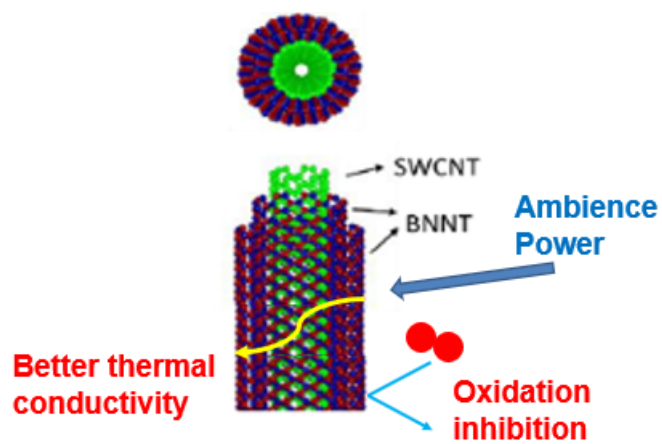
Fig. 4.5 BN shell against high power.
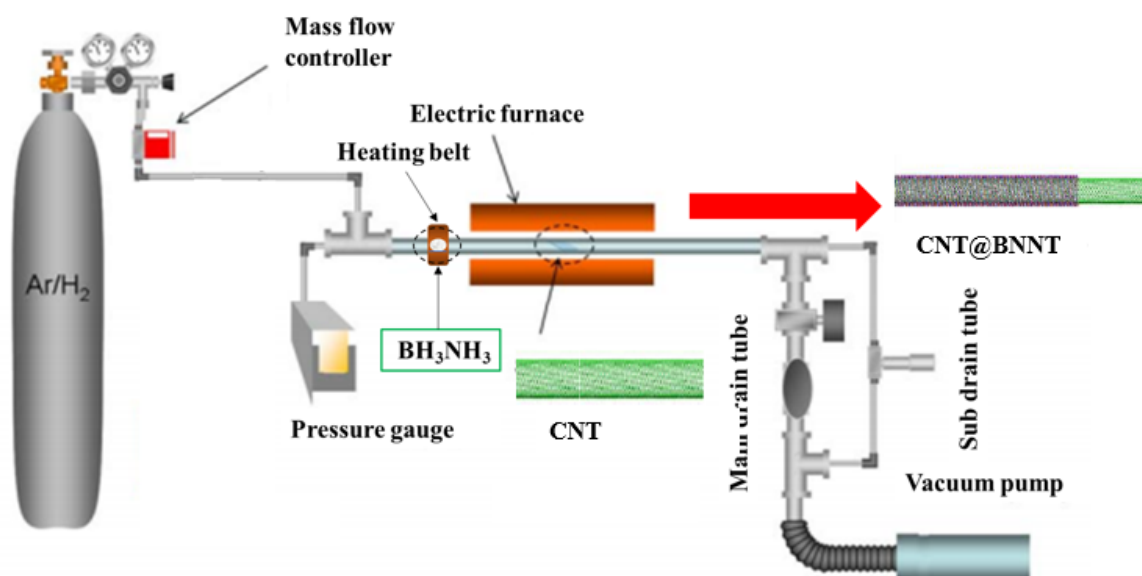
Fig. 4.6 CVD system of BN coating on CNT.

BN coating. The SWCNT film is fabricated by aerosol CVD method [41], which is then placed at the center of the electric furnance for the further synthesys. 30 mg ammonia borane (H_3NBH_3) as the BN precursor is placed at the upstream and heated to 70-90 ˚C by a heating belt. Ar with 3% H_2 as the carrier gas is flowing at a rate of 300 sccm. A low-pressure thermal CVD is required with the reaction temerature and pressure set as 1000-1100 ˚C and 300 Pa respectively. The building of BNNT follows an open-end growth mechanism [42]. The number of external BNNT walls is influenced by coating duration. In this thesis, the samples used are obtained from a 3-hour CVD. BNNTs distribute evenly along outer surfaces of most of the SWCNT. Through X-ray photoelectron spectroscopy measurement, no apparent C-N bond and B-C bond signals are observed, which indicates there is no noticeable substitution of atoms.

4.4   Optical Properties Comparison

After CNT@BNNT was synthesized, several measurements are done together with the template CNT. The absorption spectra, saturable absorber and optical damage threshold of CNT@BNNT and the template CNT are measured and compared. The results can support the idea that CNT@BNNT can substitute CNT as a saturable absorber applied in ultrafast optics with higher optical damage threshold.

4.4.1   Absorption Spectra

Fistly absorption spectra of CNT before and after BN coating was obtained in UV-vis-NIR measurement. See Fig. 4.7. The black line is the absorbance of the pristine CNT, while the red line is CNT@BNNT versus light wavelength. The absorbance peaks in visible-infrared wavelength region of the black line indicate that the CNT sample used here is a mixture of metallic and semiconducting nanotubes with average diameter of about 2.2 nm. The peak appearing in ultraviolet wavelength region is from π-plasmon resonance. The red line is close to the black line in visual and infrared region, and the three absorbance peaks show little wavelength shift and value change compared to the black curve. The high and steer slope appeared in red line near the π-plasmon resonance absorption peak is from BNNT's bandgap. ~5.5 eV is consistent with ~225 nm. This result indicates that BN coating does not influence the chirality distribution as well as low-energy-level band distribution of the inner CNT. And the external BNNTs are almost linearly transparent to infrared wavelength photons. This result can support the assumption that CNT@BNNT can perform as a saturable absorber with similar properties to CNT.
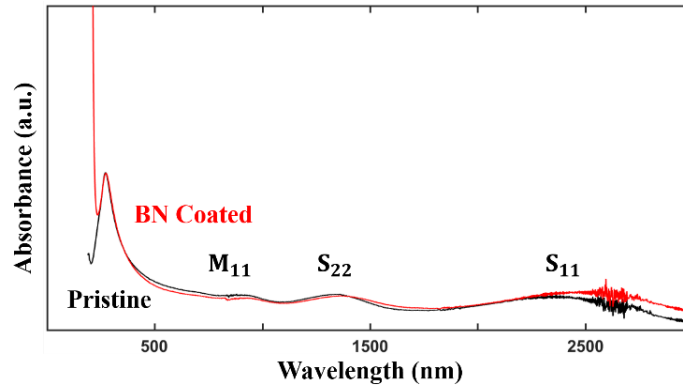
Fig. 4.7 Absorption spectra of CNT (black line) and CNT@BNNT (red line).

4.4.2   Saturable Absorption

Subsection 4.4.1 shows some indirect evidence on the existence of saturable absorption of CNT@BNNT. To confirm what influence the BN coating may bring to CNT's optical saturable absorption characteristics, absorbance versus input power are measured and compared. The experimental setup is illustrated in Fig. **??**. A mode-locked pulse fiber laser operating at 1.5 μm, generating 750-fs pulses with 50 MHz repetition rate is used as an optical source. The launched light is firstly attenuated by an electrical variable attenuator and then divided by a 9:1 fused-type fiber coupler. 90% of the light is input to hit the CNT / CNT@BNNT film sample which is adhered to and sandwiched by two fiber ferrules. Transmitted power is detected by one channel of a two-channel power meter. An attenuator with suitable attenuation is inserted between the sample and the power meter to ensure no saturation phenomenon will occur on the photon detector. Meanwhile the other channel monitors the 10% of the light to grasp the light power before hitting the sample. The input power is adjusted downward step by step in one measurement by turning down the variable attenuator. Absorbance of the samples is calculated from the data acquired from the two-channel power meter. Fig. 4.9 shows normalized absorbance dots of the samples via input pulse energy flux. The blue dots are of CNT and the red dots are of CNT@BNNT. It can be clearly seen from the graph that both CNT and CNT@BNNT appear decreasing absorbance rates versus increasing input light energy flux, which are typical saturable absorption measurement results. It confirms that BN-coating will not eliminate the saturable absorption characteristics of inner SWCNT, although it may decrease the saturation energy level, as observed from the trends of the absorbance variation. The decreased saturation power level by BN coating may be because of the less heating effect due to higher thermal conductivity.
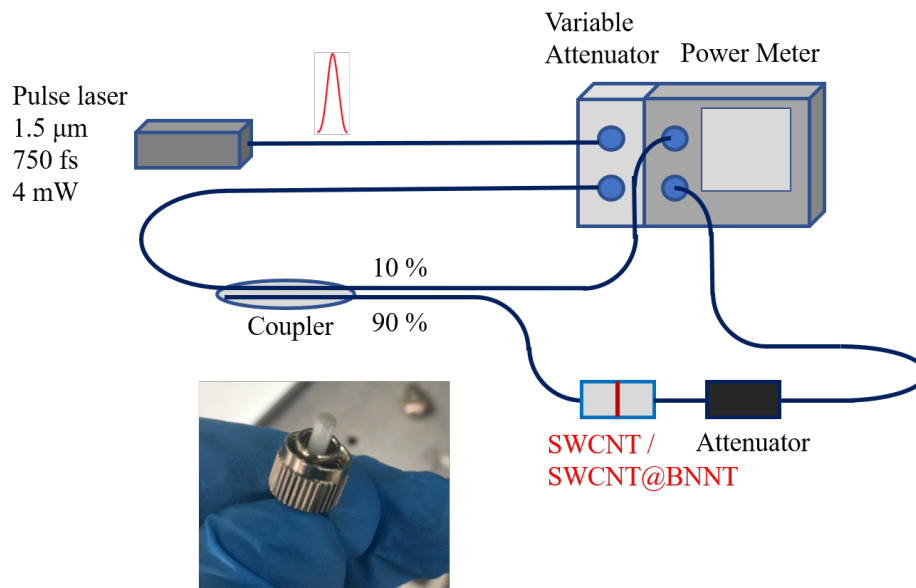
Fig. 4.8 Experimental setup of saturable absorption measurement.
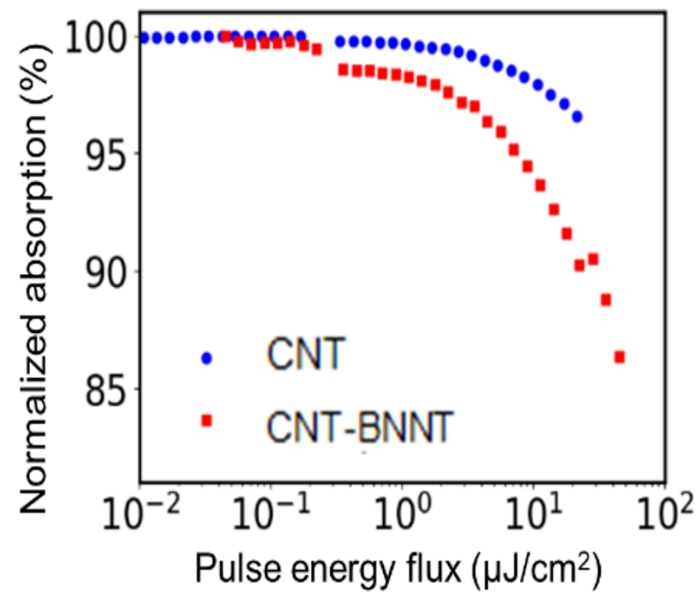
Fig. 4.9 Saturable absorption of CNT and CNT@BNNT in blue and red dots, respectively.

4.4.3   CNT@BNNT Incoporated Mode-locked Ring-cavity Laser

The nonlinear absorption is measured, then we built a simple ring-cavity faiber laser to directly prove that CNT@BNNT can act as saturable absorber. The laser scheme is shown in Fig. 4.10. A laser diode emits 980-nm pump light into the resonator through a 980/1550 wavelength division multiplexing (WDM) coupler. The CNT@BNNT film is sandwiched between two fiber ferrules. 4.5-meter-long EDF with peak absorption rate of 6 dB/m is spliced into the cavity as gain medium. And 20-meter-long SMF is spliced to compensate the normal dispersion induced from EDF. An isolator is set to prevent reflection interference. And a 90:10 coupler is used as output coupler. The result is shown in Fig. 4.11. The cavity starts mode-locking oscillation from the pump power of 13 mW. The result is taken when the pump power is 31 mW. The output power is -10 dBm. Fig. 4.11a and 4.11b show a typical soliton spectrum with full-width-half-maximum (FWHM) of 2.4 nm and a pulse train with repetition rate of 7.4 MHz which indicates a 27-meter-long resonator.

We can now ensure that CNT@BNNT can be used as saturable absorber in mode-locked fiber laser.
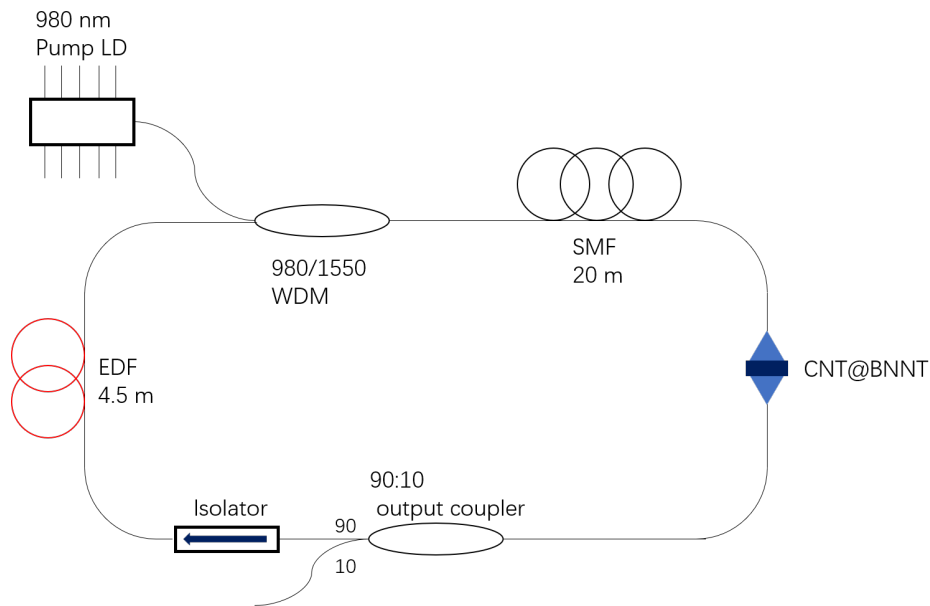
Fig. 4.10 Experiment setup of a CNT@BNNT incoporated ring-cavity fiber laser.

4.4.4   Optical Damage Threshold

After it is confirmed to that CNT@BNNT can be used in fiber laser system as saturable absorber, we measure the optical damage thresholds of CNT and CNT@BNNT. The mea-
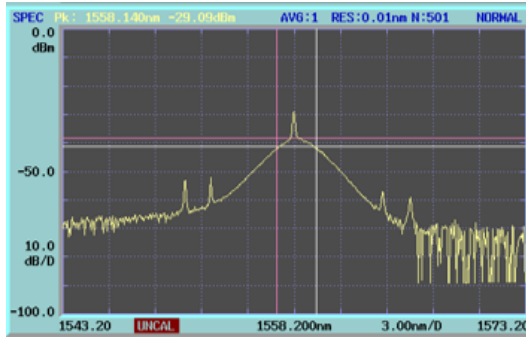
(a) Optical spectrum.
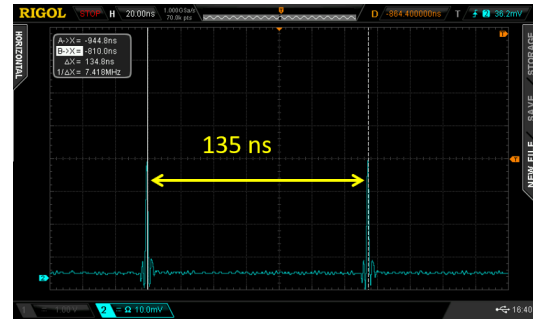
(b) Pulse train from oscilloscope.

Fig. 4.11 Results of mode-locking in CNT@BNNT incoporated ring-cavity laser.

surement schematic is shown in Fig. 4.12. Since these carbonic samples is expected to be structurally damaged and degraded to optical dust during investigating the damage threshold, samples are measured in free space rather than a fiber system in order to prevent the fiber components from burned out. A (CW) laser operating at 1.5 μm is used here as a light source. The launched light is then amplified by an Erbium doped fiber amplifier (EDFA) to a high level where is considered to exceed the mighty damage threshold of CNT@BNNT. A variable attenuator is set after the EDFA to control the input power to samples. A 9:1 fused-type fiber coupler separates the power-adjusted light into two ports. The 10% port is connected to PD 2. The input power to samples is monitored through this port. The rest 90% of the launched light is sent to free space through a collimator and focused onto the fixed sample after an aspherical lens. The beam diameter on the focus is measured as 2.6 μm by a beam profiler. The transmitted light is refocused after a Bi-convex lens and then collected by PD 1. PD 1 and PD 2 are of the same model number whose signals are processed by a two-channel power meter. Transmittance is calculated from monitored input power and transmitted power after loss compensation.

The principle of the measurement is described as follows. Step one, increase the input power to the sample from zero gradually, meanwhile the transmittance is monitored. Step two, stop increasing the input power, decrease the input power to the sample, monitoring whether the transmittance dots can trace back to the starting points. If the sample shows the same or similar transmittance at low input power before and after the high-power light is input, we judge that the sample is not irreversibly damaged yet. Then step one and two will be repeated at gradually higher power levels until the irreversible optical damage threshold is found. Comparing to saturable absorption measurement, this measurement uses a CW laser rather than a pulse laser as light source. The reason is to eliminate the strong nonlinear effect induced by ultrashort pulse.
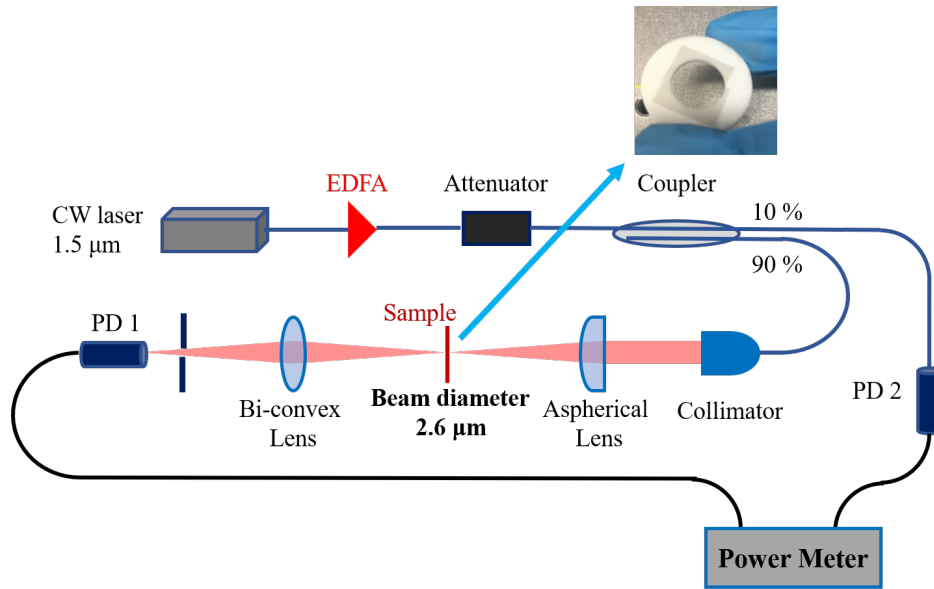
Fig. 4.12 Experimental setup of optical damage threshold measurement.

We first investigate the optical damage threshold of CNT following the principle described above. The measurement result is plotted in Fig. 4.13. The numbers indicate the measurement sequences, and the arrows show the directions of the input power variations during the measurement. Sequence 1 shows a rapid raise in transmittance from around 35 mW. Sequence 2 shows that the transmittance keeps in a higher value than before when the input power is turned downward to 10 mW. When increase the input power again from 35 mW, the transmittance shows a continuous rapid raise, as sequence 3 shows. The transmittance does not fall anymore when decrease the input power after 35 mW, as sequence 4 indicates. The irreversible damage threshold of SWCNT is clearly indicated to be around 35 mW according to measurement sequence 1 and 2, while sequence 3 and 4 appeal a deeper damage on the sample under a higher optical power hitting.

Then the same measurement is done on CNT@BNNT, as Fig. 4.14 shows. Sequence number 1 shows a group of slowly rising transmittance dots. The input power is adjusted upward gradually till 175 mW and then downward to the initial value. Sequence 2 shows when gradually adjust the input power down, the transmittance of CNT@BNNT can return to the initial value before the power adjustment. Meanwhile the backward dot trace is near the upward dot trace. This shows that the sample is still recoverable after interacting with input light. Input power is then further increased a little bit, as sequence 3 shows. Then we repeat the input-decreasing here, we found that the transmittance does not trace back, as sequence 4 shows. Sequence 3 and 4 indicate an onset of an irreversible damage around an
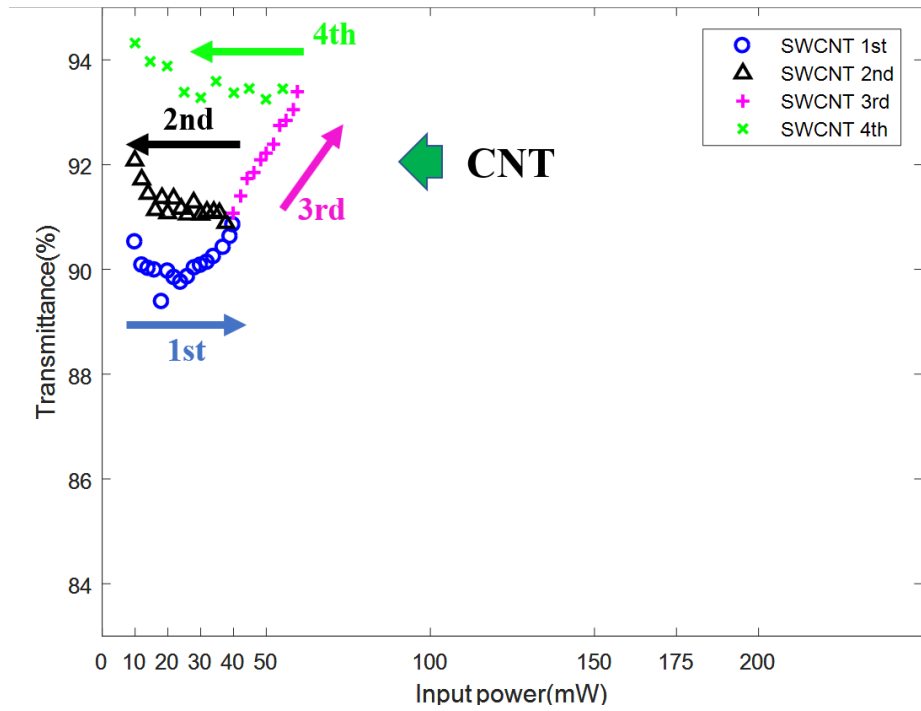
Fig. 4.13 Optical damage threshold measurement of CNT.

input power of 175 mW. The occurrence of further optical damage is shown by sequence 5 and 6.

The optical damage thresholds of CNT and CNT@BNNT are compared in Fig. 4.15. Irreversible damage occurs to CNT and CNT@BNNT at an input power of ~35 mW and ~175 mW, respectively. It is clear that BN coating can significantly improve the optical damage threshold of CNT up to 5 times that of pristine CNT. And the optical damaging rate is also reduced, this is considered to be brought from the better thermal conductivity. And since the beam diameter at focus in free space is smaller than the core diameter of single-mode fiber (~9 μm), we can reasonably expect a higher threshold value in when the material is applied in fiber system.

The photos of burn marks appeared after the damage threshold investigation are shown in Fig. 4.16. The photo is taken from optical microscope. We would like to take SEM images of these damaged samples to check how are the nanotubes damaged by light.
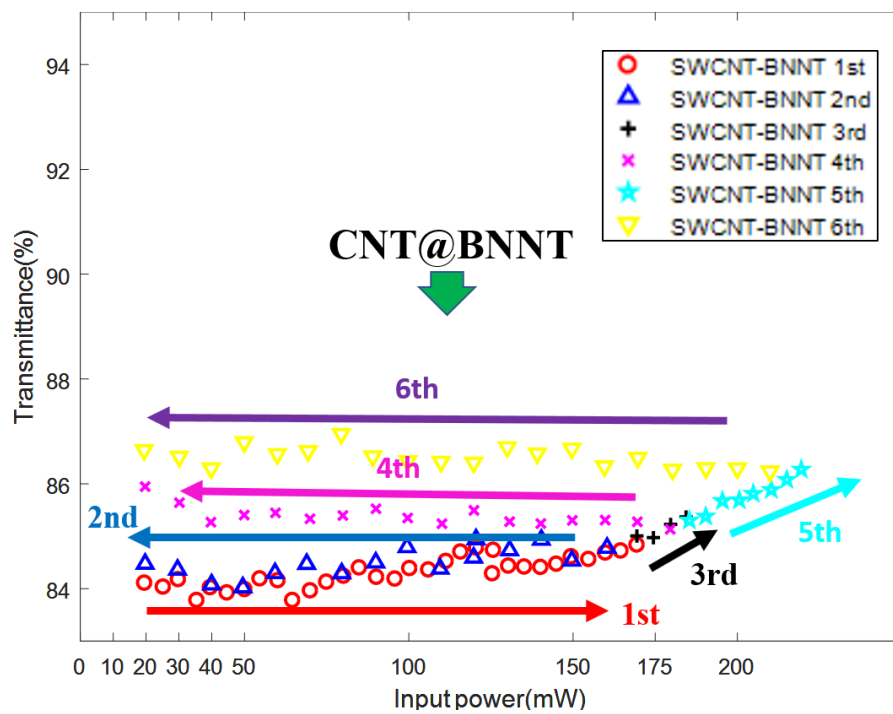
Fig. 4.14 Optical damagethreshold measurement of CNT@BNNT.
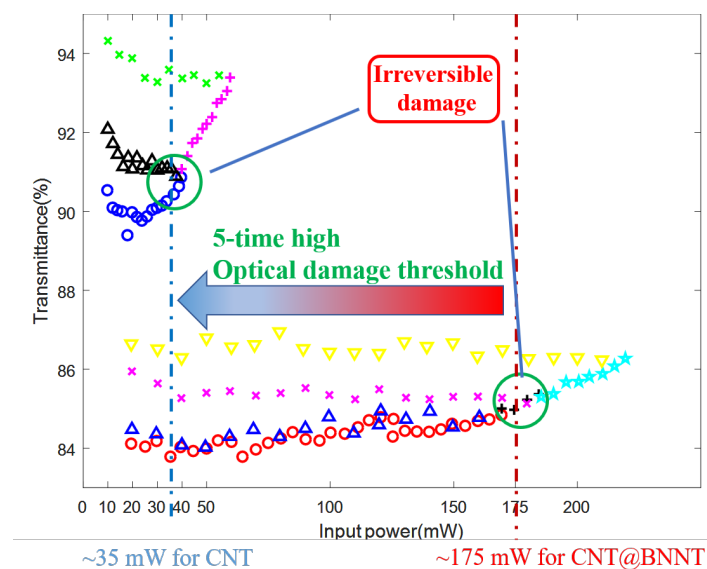
Fig. 4.15 Damage threshold comparison between CNT and CNT@BNNT.
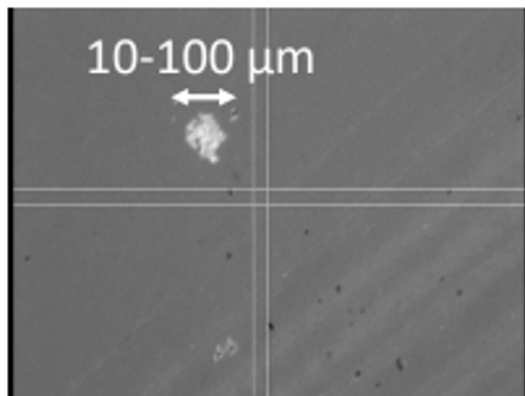
(a) Burn mark on CNT film.

(b) Burn mark on CNT@BNNT film.

Fig. 4.16 Burn marks on samples after investigating the optical damage threshold.

Chapter 5

Short Cavity Fiber Laser

In this chapter we demonstrate the attempt on short-cavity fiber laser mode-locking and dispersion management.

5.1 Short Cavity With CNT

In the early stages, we try to mode-lock fiber lasers with cavity length of 10 cm, whose net cavity dispersion distributes from small normal dispersion regime to small anomalous regime. Gain fiber used here are commercially common highly doped EDF, different from the previous researches [19, 33], which has normal chromatic dispersion. Mode-locked fiber laser at dissipative soliton or stretched pulse state is in expectations to generate pulses with higher pulse power than soliton state. CNT is firstly chosen as saturable absorber because it is super compact and easy to use, according to the previous researches.

5.1.1 CNT Spray

There are several methods to make CNT saturable absorber device, like polymer embedding method that disperses CNTs inside polymer material [43], direct synthesis method that grows nanotubes on target component [44], or optical deposition method that uses optical tweezer effect to accumulate CNTs on target part [45]. In this thesis, we firstly chose spray method to spray CNT-dispersed solvent onto target components.

We chose Dimethylformamide (DMF) as solvent, the reason is that DMF is kind of nonpolar solvent so that allows nonpolar material such as CNT to fully disperse. Meanwhile the Amide from DMF will adhere to nanotubes to help prevent the rebundle of dispersed nanotubes. We first introduce the preparation of CNT-DMF solution.
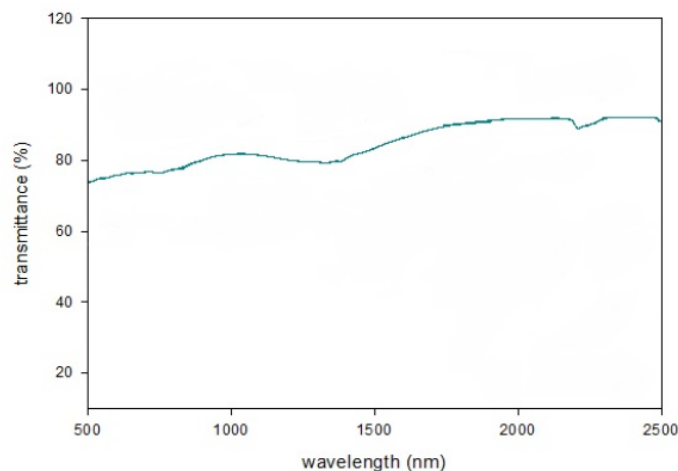
Fig. 5.1 Transmission spectrum of CNT.

First, prepare the container. The container should be prewashed by water to clean the impurity and then be washed by DMF to remove moisture. The DMF-washing is to prevent the existence of Hydroxyl in the solution which may lead to the bundle of dispersed nanotubes after long term storage.

Second, prepare the CNT solution. The CNT powder used here are made by HiPCO method, and the absorption spectrum is shown in Fig. 5.1. Take out powder weighing about 20 mg, relative to a 300 mL container. Then pour the powder into the container, after which pour DMF in. The operating should be done in windless environment.

Third, disperse nanotubes. In this thesis we used an ultrasonic cleaner to apply ultrasound oscillation to the solution. The container is placed in the cleaner which is half-filled by water, and the container is pressed tightly to cleaner's bottom by external force like tapes. The ultrasonic cleaner is set in hybrid mode. The cleaner will apply 28/45/100 Hertz ultrasound alternatively, and every frequency lasts for 15 second. One ultrasonic dispersion duration is 30 minutes. Till qualified dispersive solution obtained, it may need 2 or 3 or even more times of ultrasonic dispersion. Fig. 5.2a shows some CNT-DMF solution samples.

Fourth, spray CNT solution onto target components. We use a spray gun to "shoot" the fixed fiberferrules inside a draft chamber in a properly close distance. Meanwhile a dryer is set near the spary trajectory to heat the liquid on the way and mirror surface. See Fig. 5.2b. The spray speed is adjusted to make sure that DMF will soon evaporate after droplets reach the mirror surfaces, otherwise accumulated liquid will obstruct the futher adhesion of CNT.

Fifth, measure the linear loss of adhered CNT.

Step fourth and sixth will be repeated before the loss achieves an expectation value.
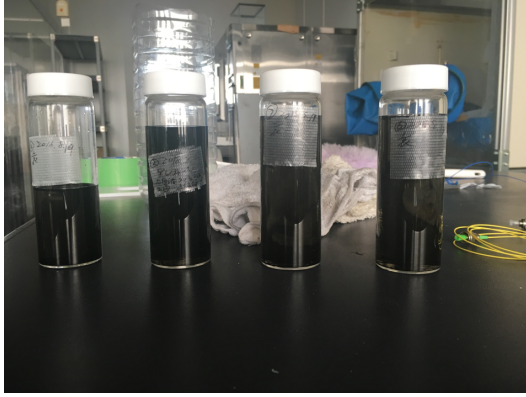
(a) CNT-DMF solution samples.
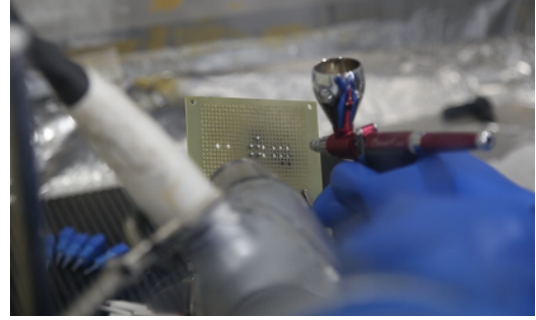
(b) Spraying in a draft chamber.

Fig. 5.2 CNT spraying.

After CNT-sprayed fibers were obtained, we firstly use a ring cavity fiber laser to verify the effectiveness of the sprayed CNT. The laser setup is shown in Fig. 5.3, which is similar to the setup in Fig. 4.10. The EDF is 2.5 meters long and SMF is around 10 meters long. A 90:10 coupler is used as output coupler. The experiment results are shown in Fig. 5.4. The mode-locking threshold of pump power is around 10 mW. The linear loss of sprayed CNT is 2 dB. Typical mode-locking results are seen from optical spectrum analyzer (OSA) and oscilloscope. The effectiveness of CNT-spraying is verified.
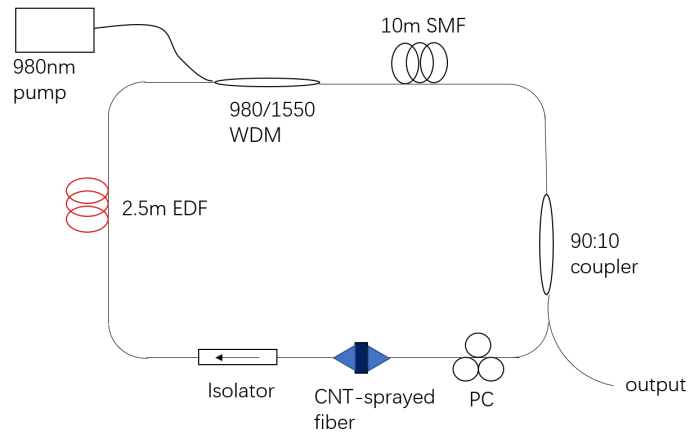
Fig. 5.3 Experimental setup of ring cavity fiber laser using CNT-sprayed fiber.

5.1.2   Experiment Result

After the verification of CNT-spraying method, we utilize this technique in short cavity fiber laser. CNT is sparyed onto a high reflection (HR) fiber ferrule type mirror which is
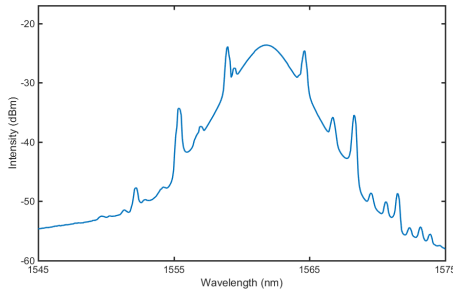
(a) Optical spectrum.
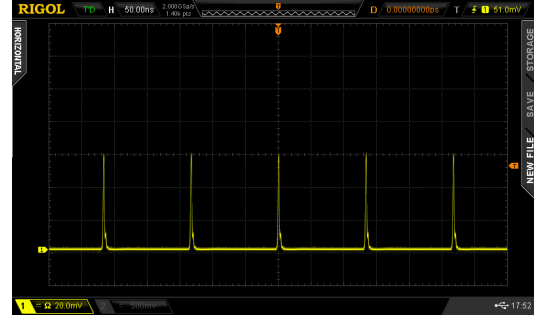
(b) Pulse train.

Fig. 5.4 Experimental result from ring cavity laser.

transparent to 980-nm-wavelength light, and then is coupled into laser cavity shown in Fig. 5.6. Pump light is emitted through a WDM coupler into the resonator that is composed by two HR mirror (R = 95%) and spliced SMF and EDF with several combinations of length (see Fig. 5.5). The resonator's total length is 10-cm-long. Isolator and angle-polished connector (APC) are used to prevent reflection interference. EDF used here is commercially available highly-doped one, with peak absorption rate of 110 dB/m. The spliced length of EDf can be chosen as 10cm, 6cm, 5cm, 4cm, 3cm.
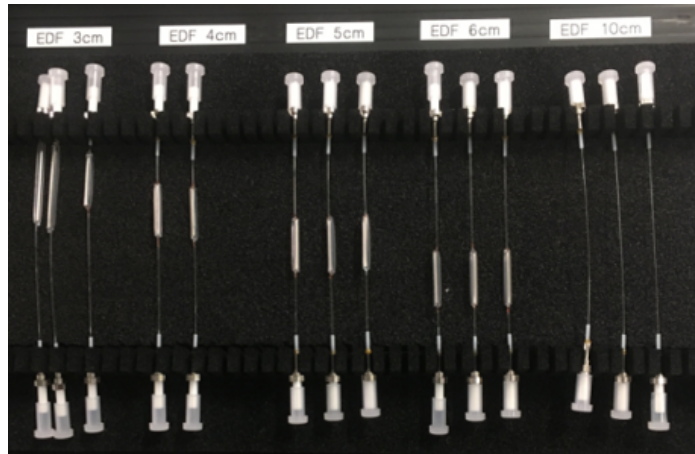
Fig. 5.5 Short cavities with different length combinations.

During the experimental attempt on mode-locking this laser, we failed to mode-lock with all the prepared cavity combinations. And we further observed that the CNT sprayed on fiber ferrule was burnt, as shown in Fig. 4.16.

The reason for burning out is that for this cavity, since the gain is so low that high pump power is needed to initiate CW and mode-locking oscillation. However, since the pump light, which will exceed 100 mW during the experiment, is inevitiblly hitting the CNT, pump

power thus will exceed the damage threshold of CNT before mode-locking starting. That is, we failed to mode-lock this short cavity fiber laser with CNT.
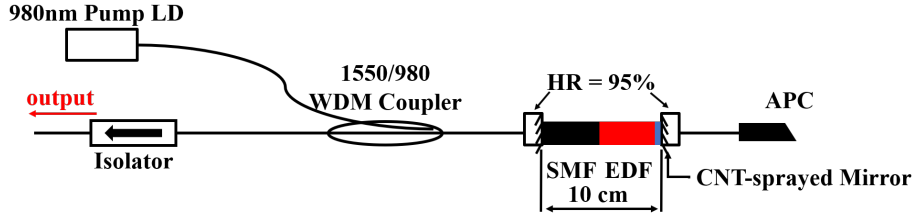
Fig. 5.6 Experimental setup of short cavity fiber laser using CNT.

To solve this problem, we thought out two solution. One is to change the laser setup, one is to change the saturable absorber with higher damage threshold. Fig. 5.7 shows one idea that using the WDM coupler to seperate gain medium and SA. In this cavity SA will only interact with signal light, which does solve the damage problem. However, limited by splice technique and the length of WDM, the cavity length is limited in a relative long level, which is quite far away from our thesis's purpose. So that changing the saturable absorber seems to be more practical. This new SA is CNT@BNNT as we introduced in chapter 4.
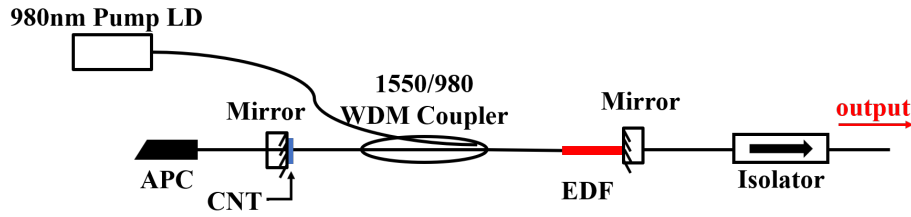
Fig. 5.7 A cavity designed to avoid SA being hit by pump light.

5.2 Short Cavity With CNT@BNNT

In chapter 4 we introduced and investigated CNT@BNNT as saturable absorber with higher damage threshold. Here we replace CNT with CNT@BNNT as new saturable absorber, as shown in Fig. 5.8. The threshold pump power for mode-locking this cavity is 180 mW.

And the experimental results are shown in Fig. 5.9. The output spectrum, oscilloscope trace, RF spectrum and autocorrelation trace are illustrated in Fig. 5.9a 5.9b 5.9c and 5.9d, respectively, at a pump power of 470mW. The SMF ($\beta_2 = -23ps^2/km$) in the cavity provides an anomalous dispersion to help mode-locking whilst the EDF has a normal dispersion ($\beta_2 =$
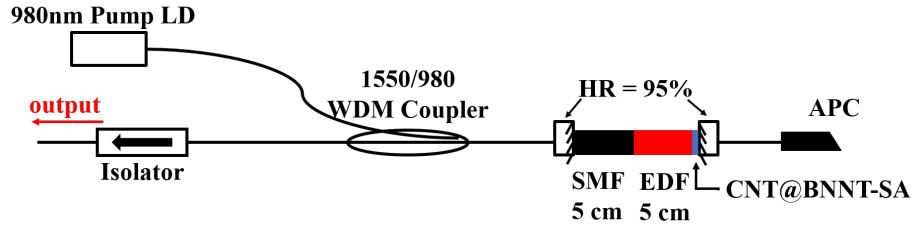
Fig. 5.8 CNT in short cavity fiber laser replaced with CNT@BNNT.

$30ps^2/km$). The net dispersion of cavity is $3.5^{-4}ps^2$. The resolution of optical spectrum is 0.01 nm. The spectral shape indicates that the pulse is stretched, with a spectral halfwidth of 6.6 nm. The oscilloscope trace shows that the output is slightly multiple pulsed since the pump power is too high. The RF spectrum, whose resolution bandwidth (RBW) and visual bandwidth (VBW) are 1 kHz, shows a repetition rate of 1.07 GHz and a S/N ratio of 50 dB. The average output power is measured to be 50 μW. After amplifying the output to 4 mW through an EDFA, the autocorrelation trace is obtained and inferred a pulse width (FWHM) of 2.0 ps, assuming a Guassian-pulse shape. This weird autocorrelation trace is resulted from multiplied pulse and low level of signal power which leads to a high sampling averaging times. The total cavity optical power including the pump- and the signal-light is 320 mW, which is at a quite high power level. CNT@BNNT shows a high-power durability inside the fiber cavity even after continuously running the laser in high pump power level for 24 hours.

(a) Optical spectrum.

(b) Pulse train.

(c) RF spectrum.

(d) Autocorrelation trace.
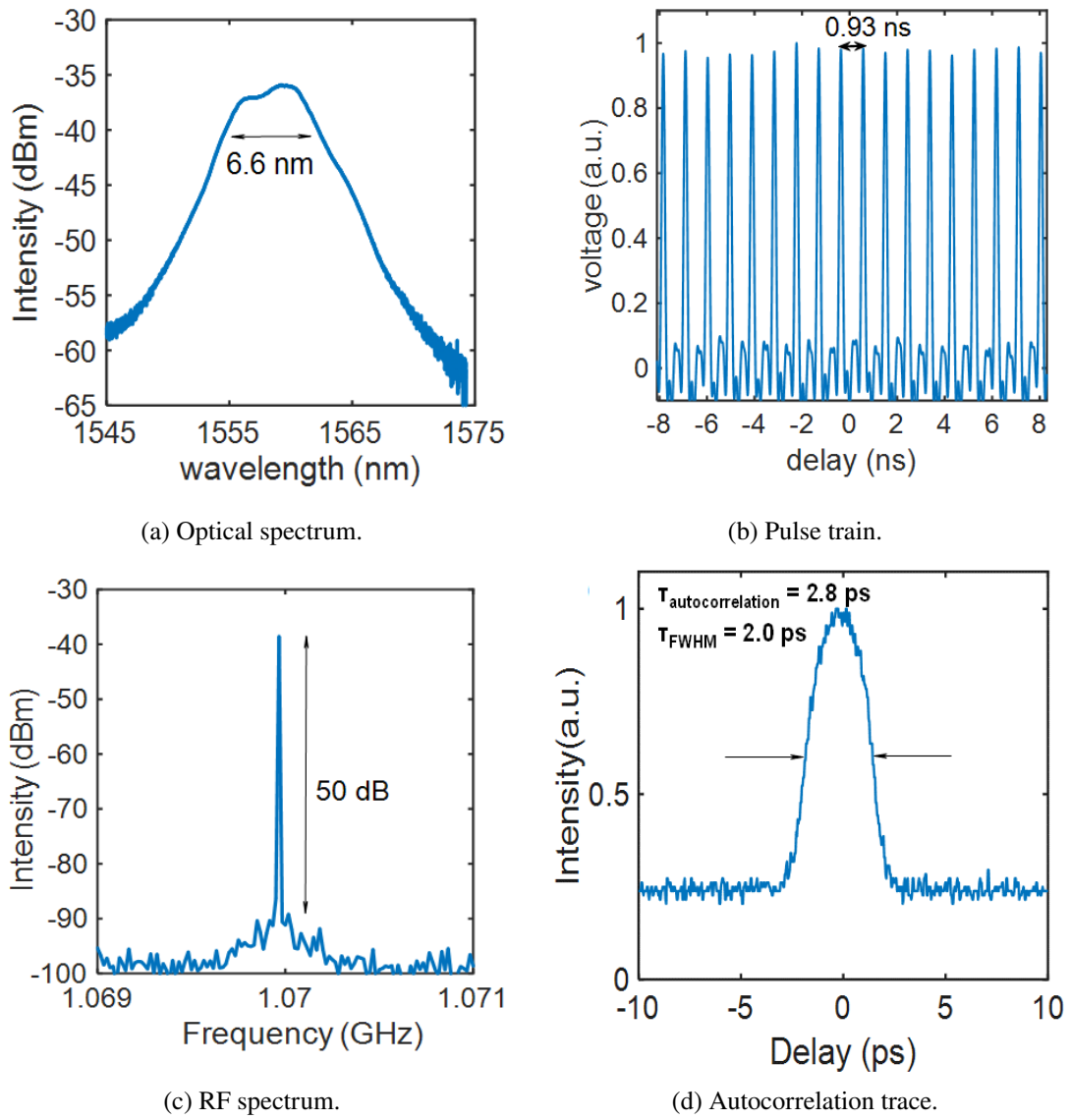
Fig. 5.9 Experimental result of 10-cm-long cavity fiber laser using CNT@BNNT.

5.3   Dispersion Management

The oscillation behavior of mode-locking is influenced significantly by GVD and SPM. Accoring to the cavity dispersion, the mode-locking oscillating region can be roughly divided into three types, they are soliton, stretched pulse and dissipative soliton.

5.3.1   Soliton, Stretched Pulse, Dissipative Soliton

Soliton

If the dispersion of the entire resonator is under anomalous dispersion, mode-locked laser oscillates in soliton state, as shown in Fig. 5.10. The SPM effect induced by pulse is counteracted by anomalous dispersion effect, so that the soliton pulse can propagate around the resonator maintaining its pulse shape stably. Fig. 5.11 is a typical output spectrum of soliton. And when the soliton pulse undergoes periodic fluctuations during the intracavity circulation, characteristic Kelly sidebands are seen in the spectrum. The fluctuations can be normal dispersion region, loss, etc. Although soliton can realize pulse propagation almost at the transform limit, the pulse energy is limited at 0.1 *nJ* level. Higher pulse energy will lead to higher SPM effect which cannot be completely cancelled by anomalous dispersion effect. Soliton pulse will then break into two or more closely spaced pulses, leading to multiple pulses in the output pulse train.
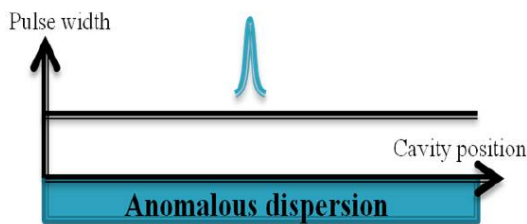
Fig. 5.10 Soliton pulse propagation.
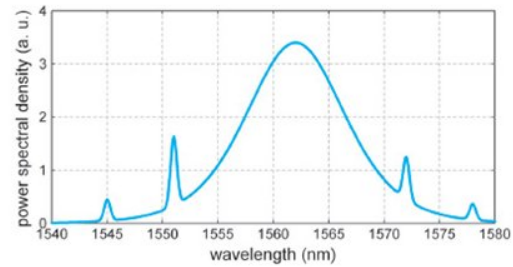
Fig. 5.11 Typical output spectrum of soliton pulse.

Stretched Pulse

If the cavity net dispersion is close to zero dispersion, mode-locked laser oscillates in stretched pulse state. As shown in Fig. 5.12, pulse travels through normal dispersion region and anomalous dispersion region alternatively and peridically, and the pulse shape experiences periodic stretch and recompression. Stretched pulses are characterized by low

phase noise because they are less affected by chirp. And as the average pulse duration in the resonator can be strongly increased, the pulse energy can be accordingly increased without obtaining excessive nonlinear phase shifts. Nanojoule energy femtosecond pulses can be generated in this way. Fig. 5.13 shows a typical output spectrum with a smooth shape of stretched pulse.
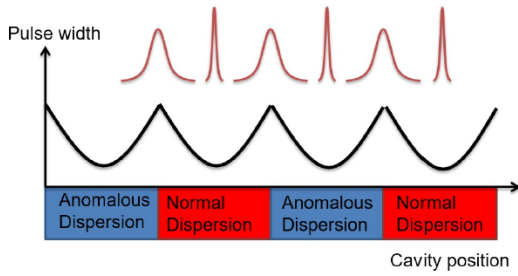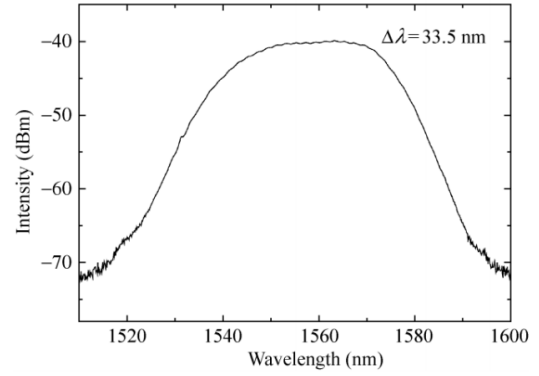

Fig. 5.12 Stretched pulse propagation.

Fig. 5.13 Typical output spectrum of stretched pulse. [46]

Dissipative Soliton

If the cavity net dispersion of the resonator is in normal dispersion region, mode-locked laser oscillates at dissipative soliton states. The pulse continues to expand its temperal width as well as spectral width due to strong chirp effect which is enhanced by overlapped SPM effect and normal dispersion effect. Then, the pulse is sharpened by an intracavity wavelength filter, or a wavelength-dependent element, and undergoes another roundtrip's chirp and amplification, as shown in Fig. 5.14. Since the pulse is strongly chirped, pulse energy can be very high (10 nJ). Moreover, through dechirp outside the cavity, pulses with ultrahigh peak power can be obtained. Fig. 5.15 shows a typical output spectrum of dissipative soliton, which has characteristic sharp side edges caused by wavelength filter effect.

5.3.2   Experimental Results

We use several different fiber cavities with different net dispersion, which are mentioned in section 5.1.2 and Fig. 5.5, to build lasers with CNT@BNNT. The laser setups are as same as Fig. 5.8. Their mode-locking behaviors are described in this subsection.
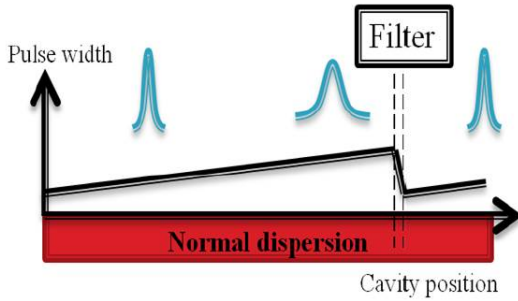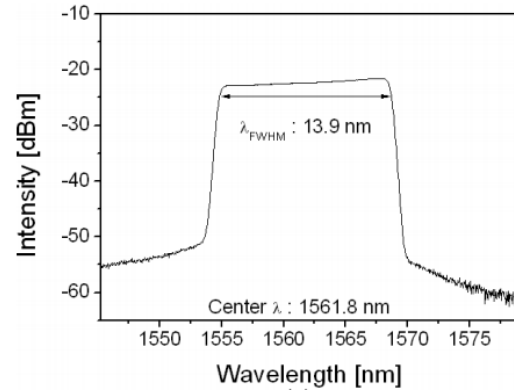
Fig. 5.14 Dissipative soliton pulse propagation.

Fig. 5.15 Typical output spectrum of dissipative soliton pulse. [47]

EDF-10cm

The fiber cavity is only composed by EDF. The net cavity dispersion is caculated as $30 \times 10^{-4} ps^2$. The laser only perfomes Q-switched mode-locking. The pulse lasing threshold pump power is 38 mW. When increasing pump power, the spectrum appears width expanding, but no phase matching is achived. Output spectrum and pulse train are obtained from OSA and oscillosopce at pump power of 155 mW, as shown in Fig. 5.16 and 5.17. The output power is 20 μW.
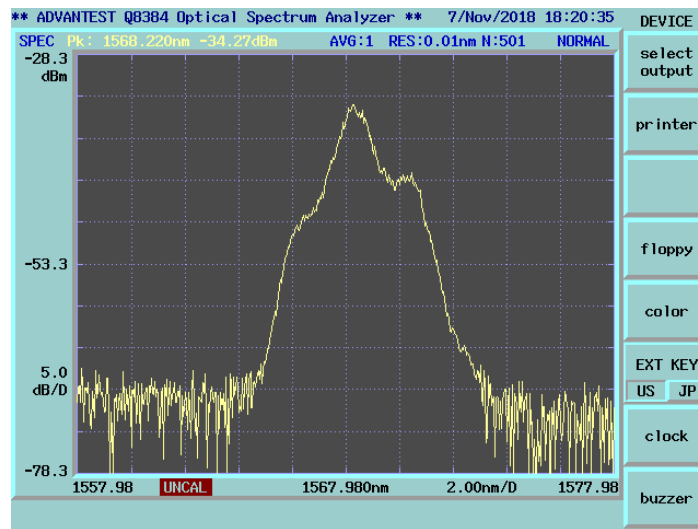
Fig. 5.16 Output spectrum.

It seens hard to mode-locking this short cavity fiber with pure gain fiber since no wavelength filter element can be induced in. So we splice SMF to realize stretched pulse mode-locking.
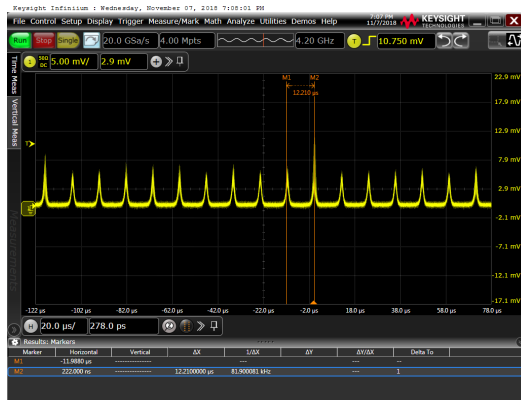
(a) Oscilloscope trace in large time scale.
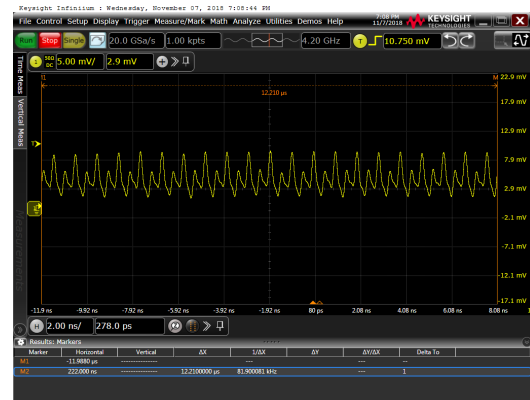
(b) Oscilloscope trace in small time scale.

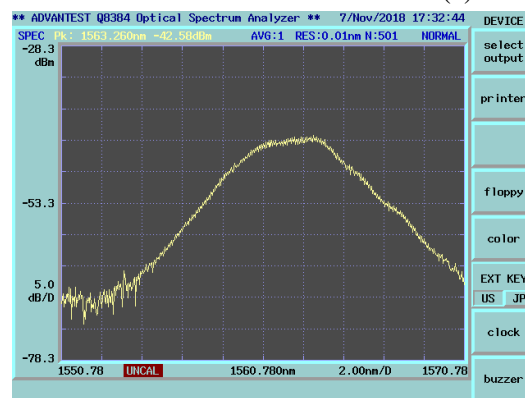Fig. 5.17 Pulse train in oscilloscope.

EDF-6cm-SMF-4cm

6-cm-long EDF and 4-cm-long SMF are spliced together. The net cavity dispersion is calculated as $8 \times 10^{-4} ps^2$. Mode-locking is achieved in this cavity. The pump power threshold is 85 mW, the FWHM is 4.48 nm, and the output at this pump level is 8 μW. The spectrum is shown in Fig. 5.18a. The output is slightly Q-switched when the pump power is near the threshold. When increase the pump power, Q-switching degrades and a stable pulse train is obtained, as shown in Fig. 5.19a and 5.19b. In spectrum, a sharp corner gruadually becomes significant as pump power increases, as shown in Fig. 5.18b. When the pump power goes beyond 168 mW, the sharp corner in spectrum disappears and ripples from multiple pulse interference show up. Multiple pulse can be seen in time domain, as shown in Fig. 5.19c.
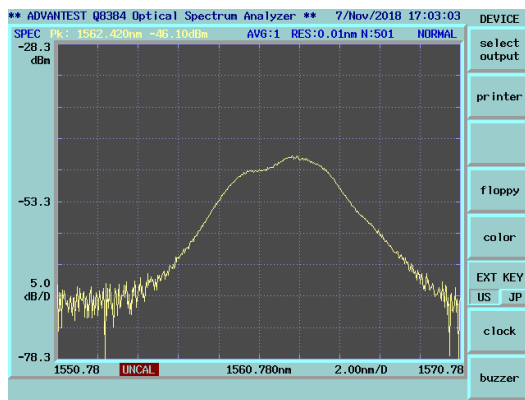
(a) Pump power of 85 mW.
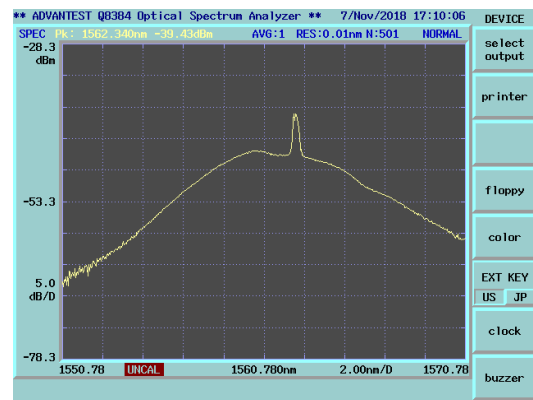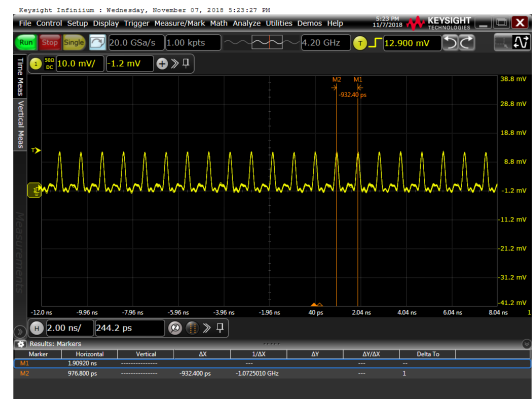

(b) Pump power of 160 mW.

(c) Pump power of 168 mW.

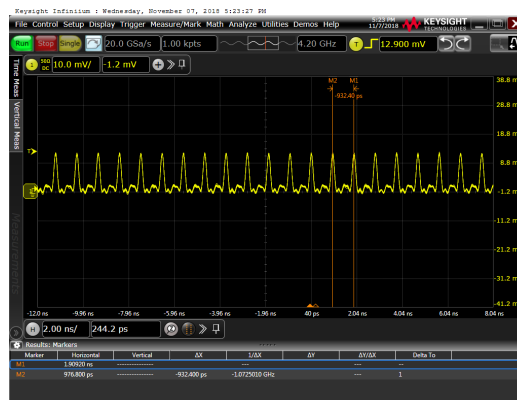Fig. 5.18 Output spectrum at different pump power.

(a) Stable mode-locked pulse train in large time scale.

(b) Stable mode-locked pulse train in small time scale.
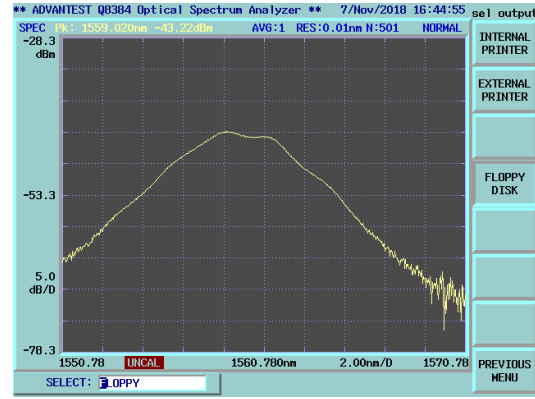

(c) Multiple pulse.

Fig. 5.19 Pulse train in oscilloscope.

EDF-5cm-SMF-5cm

5-cm-long EDF and 5-cm-long SMF are spilced together. The net cavity dispersion is calculated as $3.5 \times 10^{-4} ps^2$. Mode-locking achieved from pump power at 180 mW. Output power at threshold is 13 μW. Similar to EDF-4cm-SMF-6cm cavity, slight Q-switching near the threshold degrades when pump power increases. But no multiple pulse is observed even when the pump power is increased to 385 mW, the value which is set as upper limit. The spectra at different pump power are shown in Fig. 5.20. The FWHM is 3.12 nm.
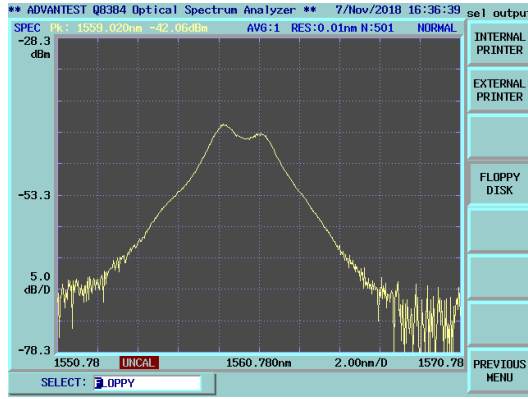
(a) Pump power of 180 mW.   (b) Pump power of 385 mW.

Fig. 5.20 Output spectrum at different pump power.

EDF-4cm-SMF-6cm

6-cm-long EDF and 4-cm-long SMF are spilced together. The net cavity dispersion is calculated as $-1.8 \times 10^{-4} ps^2$. The mode-locking threshold pump power is 280 mW. Output power is 17 μW at threshold. The laser behaves similar to the laser with EDF-5cm-SMF-5cm cavity. Slight Q-switching disappears when pump power increases, and no multiple pulse behavior is observed. The spectrum is shown in Fig. 5.21.

EDF-3cm-SMF-7cm

3-cm-long EDF and 7-cm-long SMF are spilced together. The net cavity dispersion is calculated as $-7.1 \times 10^{-4} ps^2$. For this cavity, the gain is too low to support mode-locking. The laser behavior stops at CW lasing however high the pump power is.
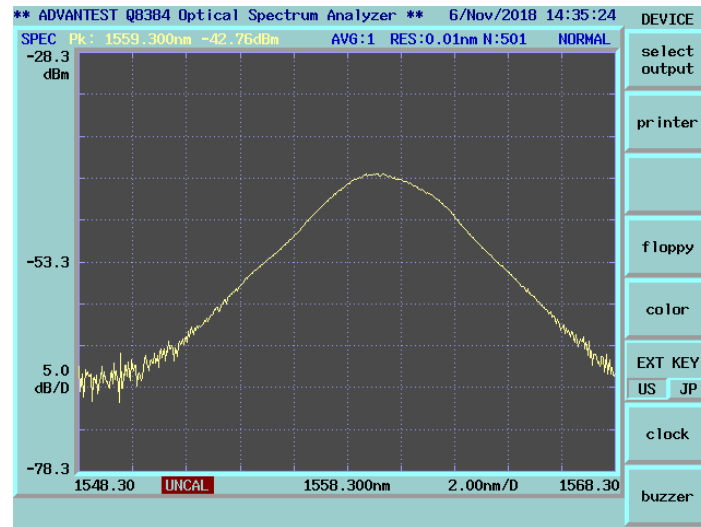
Fig. 5.21 Spectrum at pump power of 280 mW.

5.3.3   Conclusion

Lasers with same cavity length and different net cavity dispersion are demonstrated above. It seems that lasers with near-zero net cavity dispersion are able to start mode-locking. And the stable mode-locking region, which means neither Q-switching nor multiple pulse exists, is larger when the mode-locking strating threshold pump power is higher.

Chapter 6

Conclusion And Future Work

6.1 Conclusion

In this thesis, we characterize a newly developed nanomaterial, CNT@BNNT, as a kind of optical saturable absorber. Saturable absorption of CNT@BNNT is measured and compared to that of the templet CNT. The result shows that CNT@BNNT has similar saturable absorption to CNT. And its effectiveness is proved through using CNT@BNNT to mode-lock a ring-cavity fiber laser. It indicates that when CNT is wrapped concntrically by some layers of nanotubes whose bandgap is much larger than that of CNT, such as BNNT, optical absorption occuring in semiconducting CNT's bandgap will not be affected. And the optical damage thresholds of CNT and CNT@BNNT are investigated and compared. The results show that through wrapping BNNT around CNT as protective shell, the damage threshold can be improved to 5 times high when the material is used in optical system. And the optical damaging rate is also reduced, according to the better thermal conductivity. Thus we can use CNT@BNNT as saturable absorber to replace CNT in optical systems in which CNT cannot tolerent high power. In fact, CNT@BNNT can tolerent intracaviy optical power up to 320 mW and meanwhile function as saturable absorber.

CNT@BNNT in recently report is classified as one dimensional heterostructures material. This concept and technique is applicable to other materials. In this thesis we use CNT@BNNT due to BNNT's large bandgap and high thermal tolerance can protect CNT-SA. For further application, we can design and synthesize more function-designed nanomaterials. The optical application of nanomaterials, 1D or 2D, can be therefore enriched.

And we use CNT@BNNT to mode-lock 10-cm-long short cavity fiber lasers with different net cavity dispersion. Cavities with EDF length of 10cm, 6cm, 5cm, 4cm, 3cm are used, whose net cavity dispersion is $30 \times 10^{-4} ps^2$, $8 \times 10^{-4} ps^2$, $3.5 \times 10^{-4} ps^2$, $-1.8 \times 10^{-4} ps^2$ and $-7.1 \times 10^{-4} ps^2$, respectively. Cavities with EDF of 10 cm and 3 cm are failed to be

mode-locked, since the lack of anomalous dispersion and sufficient gain, respectively. The rest of cavities succeeds in stretched -pulse mode-locking. The results indicate that lasers with higher mode-locking threshold can have larger stable mode-locking region. However, all of these short-cavity lasers only produce pulses with extremely low pulse power, one of the thesis purposes to obtain high power pulse with GHz repetition rate is not realized.

6.2   Future Work

The recovery time of CNT and CNT@BNNT is not measured and compared experimentally, although we can infer that there will not be significant difference due to there is no band hybridization between CNT and BNNT. The measurement can be done in a pump-probe system. Meanwhile, the optical nolinear coefficient of CNT and CNT@BNNT can be measured and compared by Z-scan system in free space. These further measurement can help us to understand the influence brought by BNNT wrapping.

For short-cavity fiber laser, I believe if we can find a super compact wavelength filter to be added into the cavity, we can obtain high power pulse through dissipative-soliton mode-locking. And polarization maintainence cavities should also be tried, so that we can generate pulse train more stabel against enviromental vibrations.

References

[1] Abraham CS van Heel. A new method of transporting optical images without aberrations. *Nature*, 173(4392):39, 1954.

[2] HAROLD H HOPKINS and NARINDER S KAPANY. A flexible fibrescope, using static scanning. *Nature*, 173(4392):39, 1954.

[3] KC Kao and George A Hockham. Dielectric-fibre surface waveguides for optical frequencies. 113(7):1151–1158, 1966.

[4] FP Kapron, Donald B Keck, and Robert D Maurer. Radiation losses in glass optical waveguides. *Applied Physics Letters*, 17(10):423–425, 1970.

[5] William G French, John B MacChesney, PB O'connor, and GW Tasker. Bstj brief: Optical waveguides with very low losses. *The Bell System Technical Journal*, 53(5):951–954, 1974.

[6] Terenuma Miya, Y Terunuma, Tatsuya Hosaka, and Tadakazu Miyashita. Ultimate low-loss single-mode fibre at 1.55 μm. *Electronics Letters*, 15(4):106–108, 1979.

[7] Kazuo Hotate and Zuyuan He. Synthesis of optical-coherence function and its applications in distributed and multiplexed optical sensing. *Journal of Lightwave Technology*, 24(7):2541, 2006.

[8] Koji Kajiwara and Kazuo Hotate. Measurement of bragg-wavelength distribution in a long-length fiber bragg grating with high speed sampling. *Applied Physics Express*, 2(8):082401, 2009.

[9] Yosuke Mizuno, Zuyuan He, and Kazuo Hotate. Stable entire-length measurement of fiber strain distribution by brillouin optical correlation-domain reflectometry with polarization scrambling and noise-floor compensation. *Applied Physics Express*, 2(6):062403, 2009.

[10] Govind P Agrawal. Nonlinear fiber optics: its history and recent progress. *JOSA B*, 28(12):A1–A10, 2011.

[11] Akira Hasegawa and Frederick Tappert. Transmission of stationary nonlinear optical pulses in dispersive dielectric fibers. i. anomalous dispersion. *Applied Physics Letters*, 23(3):142–144, 1973.

[12] Linn F Mollenauer, Roger H Stolen, and James P Gordon. Experimental observation of picosecond pulse narrowing and solitons in optical fibers. *Physical Review Letters*, 45(13):1095, 1980.

[13] Yuya Takubo, Takuma Shirahata, and Shinji Yamashita. Optimization of a dispersion-tuned wavelength-swept fiber laser for optical coherence tomography. *Applied optics*, 55(27):7749–7755, 2016.

[14] U Keller, DAB Miller, GD Boyd, TH Chiu, JF Ferguson, and MT Asom. Solid-state low-loss intracavity saturable absorber for nd: Ylf lasers: an antiresonant semiconductor fabry–perot saturable absorber. *Optics letters*, 17(7):505–507, 1992.

[15] Ursula Keller. Recent developments in compact ultrafast lasers. *nature*, 424(6950):831, 2003.

[16] VJ Matsas, TP Newson, DJ Richardson, and David N Payne. Selfstarting passively mode-locked fibre ring soliton laser exploiting nonlinear polarisation rotation. *Electronics Letters*, 28(15):1391–1393, 1992.

[17] Sze Y Set, Hiroshi Yaguchi, Yuichi Tanaka, and Mark Jablonski. Ultrafast fiber pulsed lasers incorporating carbon nanotubes. *IEEE Journal of selected topics in quantum electronics*, 10(1):137–146, 2004.

[18] Qiaoliang Bao, Han Zhang, Yu Wang, Zhenhua Ni, Yongli Yan, Ze Xiang Shen, Kian Ping Loh, and Ding Yuan Tang. Atomic-layer graphene as a saturable absorber for ultrafast pulsed lasers. *Advanced Functional Materials*, 19(19):3077–3083, 2009.

[19] Shinji Yamashita, Yusuke Inoue, Kevin Hsu, Tomoharu Kotake, Hiroshi Yaguchi, Daisuke Tanaka, Mark Jablonski, and Sze Y Set. 5-ghz pulsed fiber fabry-pe/spl acute/rot laser mode-locked using carbon nanotubes. *IEEE Photonics Technology Letters*, 17(4):750–752, 2005.

[20] Amos Martinez and Shinji Yamashita. Multi-gigahertz repetition rate passively mode-locked fiber lasers using carbon nanotubes. *Optics express*, 19(7):6155–6163, 2011.

[21] Wadi Sulaiman and Arof Hamzah. Current developement in optical fiber technology. 2013.

[22] NJ Doran and David Wood. Nonlinear-optical loop mirror. *Optics letters*, 13(1):56–58, 1988.

[23] Martin Hofer, MH Ober, F Haberl, and ME Fermann. Characterization of ultrashort pulse formation in passively mode-locked fiber lasers. *IEEE journal of quantum electronics*, 28(3):720–728, 1992.

[24] Joonhoi Koo, Young In Jhon, June Park, Junsu Lee, Young Min Jhon, and Ju Han Lee. Near-infrared saturable absorption of defective bulk-structured wte2 for femtosecond laser mode-locking. *Advanced Functional Materials*, 26(41):7454–7461, 2016.

[25] Xiantao Jiang, Shunxiang Liu, Weiyuan Liang, Shaojuan Luo, Zhiliang He, Yanqi Ge, Huide Wang, Rui Cao, Feng Zhang, Qiao Wen, et al. Broadband nonlinear photonics in few-layer mxene ti3c2tx (t= f, o, or oh). *Laser & Photonics Reviews*, 12(2):1700229, 2018.

[26] Shinji Yamashita. A tutorial on nonlinear photonic applications of carbon nanotube and graphene. *Journal of lightwave technology*, 30(4):427–447, 2011.

[27] Shinji Yamashita. Nonlinear optics in carbon nanotube, graphene, and related 2d materials. *APL Photonics*, 4(3):034301, 2019.

[28] Jeroen WG Wilder, Liesbeth C Venema, Andrew G Rinzler, Richard E Smalley, and Cees Dekker. Electronic structure of atomically resolved carbon nanotubes. *Nature*, 391(6662):59, 1998.

[29] S Maruyama. Fullerene and carbon nanotube site.

[30] Jean-Sébastien Lauret, Christophe Voisin, Guillaume Cassabois, Claude Delalande, Ph Roussignol, Oliver Jost, and L Capes. Ultrafast carrier dynamics in single-wall carbon nanotubes. *Physical review letters*, 90(5):057404, 2003.

[31] S Reich, M Dworzak, A Hoffmann, C Thomsen, and MS Strano. Excited-state carrier lifetime in single-walled carbon nanotubes. *Physical Review B*, 71(3):033402, 2005.

[32] Kazuyuki Fuse, Amos Martinez, and Shinji Yamashita. Stability enhancement of carbon-nanotube-based mode-locked fiber laser by nitrogen sealing. In *CLEO: Science and Innovations*, page CMK5. Optical Society of America, 2011.

[33] Amos Martines and Shinji Yamashita. Multi-gigahertz repetition rate passively mode-lockedd fiber lasers using carbon nanotubes. *Optics express*, 19(7):6155–6163, 2011.

[34] Amos Martinez and Shinji Yamashita. 10 ghz fundamental mode fiber laser using a graphene saturable absorber. *Applied Physics Letters*, 101(4):041118, 2012.

[35] Andre K Geim and Irina V Grigorieva. Van der waals heterostructures. *Nature*, 499(7459):419, 2013.

[36] KS Novoselov, A Mishchenko, A Carvalho, and AH Castro Neto. 2d materials and van der waals heterostructures. *Science*, 353(6298):aac9439, 2016.

[37] Rong Xiang, Taiki Inoue, Yongjia Zheng, Akihito Kumamoto, Yang Qian, Yuta Sato, Ming Liu, Devashish Gokhale, Jia Guo, Kaoru Hisama, Satoshi Yotsumoto, Tatsuro Ogamoto, Hayato Arai, Yu Kobayashi, Hao Zhang, Bo Hou, Anton Anisimov, Yasumitsu Miyata, Susumu Okada, Shohei Chiashi, Yan Li, Jing Kong, Esko I. Kauppinen, Yuichi Ikuhara, Kazu Suenaga, and Shigeo Maruyama. One-dimensional van der waals heterostructures, 2018.

[38] Raul Arenal and Alejandro Lopez-Bezanilla. In situ formation of carbon nanotubes encapsulated within boron nitride nanotubes via electron irradiation. *Acs Nano*, 8(8):8419–8425, 2014.

[39] Angel Rubio, Jennifer L Corkill, and Marvin L Cohen. Theory of graphitic boron nitride nanotubes. *Physical Review B*, 49(7):5081, 1994.

[40] Y Xiao, XH Yan, JX Cao, JW Ding, YL Mao, and J Xiang. Specific heat and quantized thermal conductance of single-walled boron nitride nanotubes. *physical Review B*, 69(20):205415, 2004.

[41] Anna Moisala, Albert G Nasibulin, David P Brown, Hua Jiang, Leonid Khriachtchev, and Esko I Kauppinen. Single-walled carbon nanotube synthesis using ferrocene and iron pentacarbonyl in a laminar flow reactor. *Chemical Engineering Science*, 61(13):4393–4402, 2006.

[42] Yagang Yao, Chaoqun Feng, Jin Zhang, and Zhongfan Liu. "cloning" of single-walled carbon nanotubes via open-end growth mechanism. *Nano letters*, 9(4):1673–1677, 2009.

[43] S Yamashita, Y Inoue, S Maruyama, Y Murakami, H Yaguchi, M Jablonski, and SY Set. Saturable absorbers incorporating carbon nanotubes directly synthesized onto substrates and fibers and their application to mode-locked fiber lasers. *Optics letters*, 29(14):1581–1583, 2004.

[44] Aleksey G Rozhin, Youichi Sakakibara, Madoka Tokumoto, Hiromichi Kataura, and Yohji Achiba. Near-infrared nonlinear optical properties of single-wall carbon nanotubes embedded in polymer film. *Thin Solid Films*, 464:368–372, 2004.

[45] Ken Kashiwagi, Shinji Yamashita, and Sze Yun Set. In-situ monitoring of optical deposition of carbon nanotubes onto fiber end. *Optics express*, 17(7):5711–5715, 2009.

[46] Zhipei Sun, Tawfique Hasan, Fengqiu Wang, Aleksey G Rozhin, Ian H White, and Andrea C Ferrari. Ultrafast stretched-pulse fiber laser mode-locked by carbon nanotubes. *Nano Research*, 3(6):404–411, 2010.

[47] Ju Hee Im, Sun Young Choi, Fabian Rotermund, and Dong-Il Yeom. All-fiber er-doped dissipative soliton laser based on evanescent field interaction with carbon nanotube saturable absorber. *Optics express*, 18(21):22141–22146, 2010.

Acknowledgements

Publication and Presentation List

1. Pengtao Yuan, Zheyuan Zhang, Shoko Yokokawa, Yongjia Zheng, Lei Jin, Sze Yun Set, Shigeo Maruyama and Shinji Yamashita, "High Power Tolerant SWCNT-BNNT Saturable Absorber for Laser Mode-Locking," Conference of Lasers and Electro-optics (CLEO) 2019, no. DF30.4, San Jose, USA, May 5-10, 2019.(Oral)

2. Pengtao Yuan, Zheyuan Zhang, Shoko Yokokawa, Yongjia Zheng, Lei Jin, Sze Yun Set, Shigeo Maruyama and Shinji Yamashita,"High-optical-power durable saturable absorber based on SWCNT-BNNT," Nano Korea 2019, no. O1902_0314, Goyang, Korea, July 3-5, 2019.(Oral)

3. 袁鵬涛，セットジイヨン，山下真司，　"モード同期線形短共振器ファイバーレーザーの分散制御"，レーザー学会第 525 回研究会「ファイバレーザー技術学会」，　名古屋大学，名古屋，　2018 年 11 月 16 日．(Poster)

4. 袁鵬涛、張哲元、横川翔子、鄭永嘉、金磊、セットジイヨン、丸山茂雄、山下真司，"高出力耐性 CNT-BNNT 可飽和吸収体を用いたモード同期ファイバーレーザ"，第 66 回応用物理学会春季学術講演会，東京工業大学大岡山キャンパス，東京，no.10p-PB5-13，2019 年 3 月 9-12 日．(Poster)